

Leveraging the Bias-Variance Tradeoff in Quantum Chemistry for Accurate Negative Singlet-Triplet Gap Predictions: A Case for Double-Hybrid DFT

Atreyee Majumdar¹, Raghunathan Ramakrishnan^{1,*}

¹*Tata Institute of Fundamental Research, Hyderabad 500046, India*

**Corresponding author: ramakrishnan@tifrh.res.in*

Abstract

Molecules that violate Hund’s rule—having first excited singlet state (S_1) below the triplet state (T_1)—are rare yet promising as efficient light emitters. Their high-throughput identification demands exceptionally accurate excited-state modeling to minimize false positives and negatives. Benchmarking twelve S_1 – T_1 energy gaps, we find that local variants of ADC(2) and CC2 deliver excellent accuracy and speed for screening medium-sized molecules. Notably, while double-hybrid DFT approximations (e.g., B2GP-PLYP and PBE-QIDH) exhibit high mean errors (> 100 meV) despite very low standard deviations (≈ 10 meV), exploring their parameter space reveals that a configuration with 75% exchange and 55% correlation reduces the mean error to below 5 meV—albeit with increased variance. Using this low-bias parameterization as an internal reference, we correct the systematic error while maintaining low variance, effectively combining the strengths of both low-bias and low-variance DFT parameterizations to enhance overall accuracy. Our findings suggest that low-variance DFT methods—often overlooked due to high bias—can serve as reliable tools for predictive modeling in first-principles molecular design.

1 Introduction

The energy criterion for organic light-emitting diodes (OLEDs) to operate via thermally activated delayed fluorescence (TADF) is that the energy of the first excited singlet state (S_1) must be no more than 0.1 eV higher than that of the triplet state (T_1)[\[1, 2\]](#). This condition facilitates thermally-aided reverse intersystem crossing (RISC), enabling the theoretical complete transfer of the T_1 population to the emissive state, S_1 [\[3\]](#). A derivative of the triangular molecule, heptazine (aka heptaazaphenylene, 7AP), with a central

nitrogen (N) atom in an anti-aromatic 12-annulene framework, showed delayed fluorescence without thermal assistance, indicating a negative S_1-T_1 gap (STG)[4]. This mechanism paves the way for designing OLEDs that leverage exothermic delayed fluorescence from inverted singlet and triplet excited states (DFIST). Direct spectroscopic evidence of a negative STG (-0.047 ± 0.007 eV) was obtained for pentaazaphenylene (5AP) using anion photoelectron spectroscopy and fluorescence measurements [5]. Negative STG was also observed in the transient photoluminescence spectrum of dialkylamine-substituted 5AP[6]. Computational studies have further suggested that azaphenalenenes (APs) with other substitution patterns, as well as the boron (B) analog of azaphenylene (1AP), boraphenylene (1BP), also exhibit negative STGs[7, 8, 9, 10, 11, 12, 13, 14]. Non-alternant hydrocarbons and their substituted analogs show the potential for negative STGs[15, 16, 17, 18, 19]. Notably, substituted analogs of the non-fused bicyclic hydrocarbon have demonstrated negative STGs, attributed to through-bond charge-transfer states[20].

A comprehensive search across 12,880 structurally diverse small molecules revealed no exceptions to Hund’s rule, indicating that achieving the electronic structure criteria for $STG < 0$ requires nontrivial molecular structures[21]. Moreover, the typical magnitudes of negative STGs are much smaller or similar to the average errors associated with popular quantum chemistry and density functional theory approximations (DFAs). Consequently, due to the rarity of molecules with negative STGs and the limitations of current quantum chemical approximations, accurately identifying molecules exhibiting $STG < 0$ via high-throughput screening—with minimal false-positive and false-negative predictions—remains challenging. The linear-response time-dependent density functional theory (LR-TD-DFT) formalism provides qualitative accuracy—*i.e.*, gets the sign of the STG for DFIST candidates correct—only within the double-hybrid (dh) DFT framework containing many-body correlation via the second-order perturbation theory (MP2). With the right combination of ingredients, dh-DFT can reliably predict a wide range of molecular properties[22, 23, 24, 23]. Nevertheless, selecting suitable exchange-correlation (XC) functionals within the dh-DFT framework remains challenging, especially for novel problems lacking sufficient reference data.

We present a scheme that leverages the bias-variance tradeoff in the dh-DFT formalism. We evaluate various computational methods for predicting twelve STGs in triangular molecules, benchmarking them against previously reported theoretical best estimates[14]. We examine dh-DFAs exhibiting very low variance for STG predictions, and reparametrize them to minimize the bias. These optimal low-bias models are used as internal references to correct the predictions of the low-variance models. This internally referenced scaling approach is demonstrated by predicting STGs with low bias and low variance, resulting in excellent overall accuracy. We discuss the merits and drawbacks of this approach for its further applications.

2 Dataset and Computational Methods

We consider twelve systems (see Figure 1) using equilibrium geometries from Ref. [14], determined at the CCSD(T) level with the frozen core approximation and the cc-pVTZ basis set. Using these geometries, we performed single-point excited state calculations with various methods. In addition, we collected TBE of the S_1 and T_1 energies from Ref. [14] to serve as reference values for benchmarking. As stated in Ref. [14], structure 11 in Figure 1 (with D_{3h} symmetry) corresponds to a saddle point on the potential energy surface at the MP2/6-311G(*d,p*) level, whereas the minimum energy geometry exhibits C_{3h} symmetry (structure 12). Similarly, a separate study[25] found that the high-symmetry forms of structures 6, 7, and 8 are not true minima and structure 2 is a very shallow potential well at the CCSD(T)/cc-pVTZ level[25]. Overall, four of the twelve structures are transition states; however, we include them in our benchmarking of STGs due to the availability of TBE-level results and the lack of alternative high-quality data.

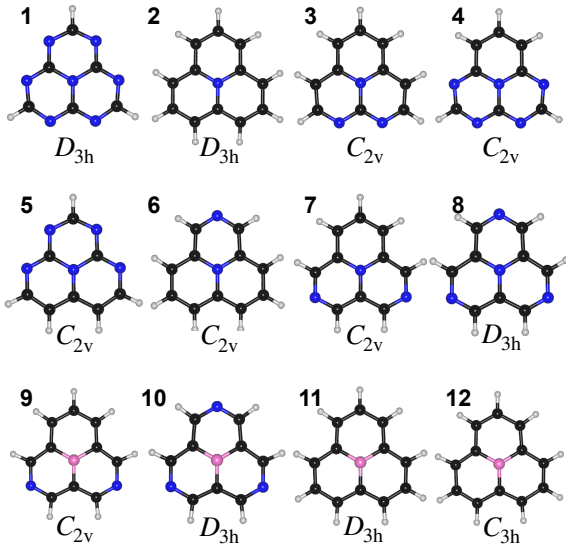


Figure 1: Nitrogen- and boron-centered [12]-annulene systems reported in Ref. [14].

Laplace-transformed, density-fitted, local versions of correlated methods—CC2 [26] and ADC(2) [27]—offer attractive speedups for modeling excited states of medium-sized molecules. We denote these methods as L-CC2 and L-ADC(2), and performed calculations with the cc-pVDZ, aug-cc-pVDZ, cc-pVTZ, and aug-cc-pVTZ basis sets, using the corresponding JKFIT and MP2FIT auxiliary basis sets. L-CC2 and L-ADC(2) are the same methods denoted as LT-DF-CC2 and LT-DF-ADC(2) elsewhere. L-CC2 and L-ADC(2) calculations were conducted using Molpro (version 2015.1) [28]. L-CC2 has been shown to deviate from the canonical variant CC2 by ≤ 0.05 eV, irrespective of the character of the excited states, including that of charge-transfer states for which CC2 can have huge error [29]. The systems studied in this work do not have charge-transfer characteristics, hence CC2 delivers good accuracy for STGs in agreement with TBEs[14]. L-CC2 has

demonstrated excellent accuracy in modeling the excited states of BODIPY derivatives [30, 31]. For comparison, we collected S_1 and T_1 energies obtained using the linear-response coupled-cluster methods, EOM-CCSD and CC3, with the aug-cc-pVDZ basis set from Ref. [14]. Additionally, we performed ADC(2) calculations using the cc-pVDZ, cc-pVTZ, aug-cc-pVDZ, and aug-cc-pVTZ basis sets with the resolution-of-the-identity (RI) approximation [32, 33] as implemented in QChem (version 6.0.2) [34].

We conducted LR-TD-DFT calculations using the Tamm–Dancoff approximation (TDA). Although TDA may not predict oscillator strengths as accurately as the random-phase approximation (RPA), RPA predictions of triplet energies are sensitive to triplet stability [35]. Therefore, TDA is preferred for automated high-throughput calculations, and previous work has shown that its STG predictions for azaphenalenenes are more accurate than that of RPA[21]. The performance of various DFAs for predicting STGs in azaphenalenenes has been discussed in prior studies [36, 37, 38].

This study explores several DFAs spanning all levels of the Jacob’s ladder [39], namely, local density approximation (LDA): VWN5 [40] and PWLDA; generalized gradient approximation (GGA): BP86, BLYP, PW91 [41, 42], PBE [43], mPWPW, and mPWLYP; hybrid GGA: B3LYP [44], PBE0 [45], X3LYP [46], mPW1PW, mPW1LYP, and BHandHLYP [47]; meta-GGA: TPSS [48], TPSSh [48], TPSS0 [48], and M06L [49] hybrid meta-GGA: M062X [50]; range-separated hybrids: ω B97, [51] ω B97X, [51] ω B97X-D3, CAM-B3LYP [52], LC-BLYP [53], and LC-PBE [54]; double hybrid: ω B97X-2 [55], B2PLYP [56], mPW2PLYP [57], B2GP-PLYP [58], PWPB95 [23], PBE-QIDH [59], PBE0-DH [60], ω B2PLYP [61], ω B2GP-PLYP [61], ω B88PP86 [62], ω PBEP86 [62], SCS/SOS-B2PLYP21 [62], SCS-PBE-QIDH [62], SCS-B2GP-PLYP21 [62], SOS-B2GP-PLYP21 [62], SCS- ω B2GP-PLYP21 [62], SOS- ω B2GP-PLYP21 [62], SCS-RSX-QIDH [62], SOS-RSX-QIDH [62], SCS- ω B88PP86 [62], SOS- ω B88PP86 [62], SCS- ω PBEP86 [62], SOS- ω PBEP86 [62], DSD-BLYP [63], DSD-PBEP86 [63], DSD-PBEB95 [63], RSX-QIDH [64], and RSX-OH [65]. All DFT calculations were performed using Orca (version 6.0.0) [66, 67].

3 Bias Correction for Low-Variance Predictors

We examine the conditions under which regression-based bias correction is effective, to correct a low-variance, high-bias predictor using a low-bias, high-variance predictor. We clarify when and how the transformation preserves variance while ensuring bias reduction.

Definitions: We begin by defining the key error metrics and terms used in this study.

1. Let \hat{y}_1 and \hat{y}_2 denote two predictive models (or predictors) for a given property. In this study, they represent two parameterizations of a DFA used for determining STG. Further, \hat{y}_{true} represents the exact theoretical value of the property under consideration. The best available finite-data estimate of \hat{y}_{true} is denoted as the

reference value, \hat{y}^{ref} . The k -th prediction from \hat{y}_1 and the corresponding reference value are denoted as $\hat{y}_{1,k}$ and $\hat{y}_{\text{ref},k}$, respectively.

2. The expected value (*i.e.*, mean) of \hat{y}_1 is given by $\mathbb{E}[\hat{y}_1]$. The variance of \hat{y}_1 around its mean is defined as: $\text{Var}(\hat{y}_1) = \mathbb{E}[\hat{y}_1^2] - \mathbb{E}[\hat{y}_1]^2$. The covariance between two predictors measures their linear relationship and is defined as: $\text{Cov}(\hat{y}_1, \hat{y}_2) = \mathbb{E}[\hat{y}_1\hat{y}_2] - \mathbb{E}[\hat{y}_1]\mathbb{E}[\hat{y}_2]$.
3. The error metrics are defined as follows. Mean signed error (MSE): $\text{MSE}(\hat{y}_1) = \mathbb{E}[\hat{y}_1 - \hat{y}_{\text{ref}}]$, mean absolute deviation (MAD): $\text{MAD}(\hat{y}_1) = \mathbb{E}[|\hat{y}_1 - \hat{y}_{\text{ref}}|]$, standard deviation of error (SDE) for a sample of size N : $\text{SDE}(\hat{y}_1) = \sqrt{\frac{1}{N-1} \sum_{k=1}^N (\hat{y}_{1,k} - \hat{y}_{\text{ref},k})^2}$. In the limit of a large sample (*i.e.*, for a population), the square of SDE corresponds to the variance.
4. The term ‘bias’ refers to a systematic shift in a distribution and requires a reference for comparison. Throughout this study, bias specifically refers to systematic shifts in prediction error: $\hat{y}_1 - \hat{y}_{\text{ref}}$. Similarly, we distinguish between: $\text{Var}(\hat{y}_1)$ and $\text{Var}(\hat{y}_1 - \hat{y}_{\text{ref}})$, where the former indicates spread around the mean value of \hat{y}_1 while latter quantifies the spread of its prediction errors, which is the primary focus of this study.

Bias Correction via Ordinary Least Squares Regression: The bias correction scheme applies in cases where two predictors, \hat{y}_1 and \hat{y}_2 , are available with known bias and variance relative to the reference values, \hat{y}^{ref} . We assume that \hat{y}_1 has low variance in prediction errors (*i.e.*, small SDE) but high bias (*i.e.*, large magnitude of MSE), and \hat{y}_2 has low bias but high variance in prediction errors. These conditions are expressed as:

$$|\mathbb{E}[\hat{y}_1 - \hat{y}^{\text{ref}}]| > 0, \text{Var}(\hat{y}_1 - \hat{y}^{\text{ref}}) \approx 0; \quad \mathbb{E}[\hat{y}_2 - \hat{y}^{\text{ref}}] \approx 0, \text{Var}(\hat{y}_2 - \hat{y}^{\text{ref}}) > 0. \quad (3.1)$$

We define a new estimator \hat{y}_1^* by linearly scaling \hat{y}_1 :

$$\hat{y}_1^* = a\hat{y}_1 + b, \quad (3.2)$$

where a and b are determined via ordinary least squares regression, minimizing the squared error with respect to \hat{y}_2 :

$$\min_{a,b} \sum_i (a\hat{y}_{1,i} + b - \hat{y}_{2,i})^2. \quad (3.3)$$

The optimal values of a and b are given by:

$$a = \frac{\text{Cov}(\hat{y}_1, \hat{y}_2)}{\text{Var}(\hat{y}_1)}; \quad b = \mathbb{E}[\hat{y}_2] - a\mathbb{E}[\hat{y}_1]. \quad (3.4)$$

Error analysis: We want to determine whether the bias and variance of \hat{y}_1^* match those of \hat{y}_2 and \hat{y}_1 , respectively. The mean of \hat{y}_1^* is:

$$\mathbb{E}[\hat{y}_1^*] = \mathbb{E}[a\hat{y}_1 + b] = a\mathbb{E}[\hat{y}_1] + b. \quad (3.5)$$

Substituting the expression for b from Eq. 3.4, we find:

$$\mathbb{E}[\hat{y}_1^*] = a\mathbb{E}[\hat{y}_1] + \mathbb{E}[\hat{y}_2] - a\mathbb{E}[\hat{y}_1] = \mathbb{E}[\hat{y}_2]. \quad (3.6)$$

Thus, least-squares regression guarantees that the mean of \hat{y}_1^* aligns with that of the reference—low-bias predictor \hat{y}_2 —ensuring that the bias is corrected. The MSE of \hat{y}_1^* follows:

$$\begin{aligned} \mathbb{E}[\hat{y}_1^* - \hat{y}^{\text{ref}}] &= \mathbb{E}[a\hat{y}_1 + b - \hat{y}^{\text{ref}}] = \mathbb{E}[a\hat{y}_1] + \mathbb{E}[b] - \mathbb{E}[\hat{y}^{\text{ref}}] \\ &= \mathbb{E}[a\hat{y}_1] + (\mathbb{E}[\hat{y}_2] - a\mathbb{E}[\hat{y}_1]) - \mathbb{E}[\hat{y}^{\text{ref}}] \\ &= \mathbb{E}[\hat{y}_2] - \mathbb{E}[\hat{y}^{\text{ref}}] = \mathbb{E}[\hat{y}_2 - \hat{y}^{\text{ref}}]. \end{aligned} \quad (3.7)$$

Hence, the MSE of \hat{y}_1^* is identical to that of \hat{y}_2 , confirming that bias is fully transferred from \hat{y}_2 .

The variance of \hat{y}_1^* follows:

$$\text{Var}(\hat{y}_1^*) = \text{Var}(a\hat{y}_1 + b) = a^2\text{Var}(\hat{y}_1). \quad (3.8)$$

For \hat{y}_1^* to preserve the variance of \hat{y}_1 , we require $a^2 = 1$, which implies $a = \pm 1$. For $a \approx 1$, \hat{y}_1^* retains the variance of \hat{y}_1 while aligning its mean with $\mathbb{E}[\hat{y}_2]$, effectively shifting the prediction distribution. However, in most practical cases, $|a| \neq 1$, leading to: $|a| < 1$ resulting in $\text{Var}(\hat{y}_1^*) < \text{Var}(\hat{y}_1)$, or $|a| > 1$ resulting in $\text{Var}(\hat{y}_1^*) > \text{Var}(\hat{y}_1)$. The variance of $\hat{y}_1^* - \hat{y}^{\text{ref}}$ is given by:

$$\text{Var}(\hat{y}_1^* - \hat{y}^{\text{ref}}) = \text{Var}(a\hat{y}_1 + b - \hat{y}^{\text{ref}}). \quad (3.9)$$

Applying the variance sum formula, $\text{Var}(A + B) = \text{Var}(A) + \text{Var}(B) + 2\text{Cov}(A, B)$, we arrive at:

$$\begin{aligned} \text{Var}(\hat{y}_1^* - \hat{y}^{\text{ref}}) &= \text{Var}(a\hat{y}_1) + \text{Var}(b - \hat{y}^{\text{ref}}) - 2\text{Cov}(a\hat{y}_1, b - \hat{y}^{\text{ref}}) \\ &= \text{Var}(a\hat{y}_1) + \text{Var}(\hat{y}^{\text{ref}}) - 2\text{Cov}(a\hat{y}_1, \hat{y}^{\text{ref}}) \\ &= \text{Var}(a\hat{y}_1 - \hat{y}^{\text{ref}}) \\ &= a^2\text{Var}(\hat{y}_1 - \hat{y}^{\text{ref}}/a). \end{aligned} \quad (3.10)$$

This implies that the variance of $\hat{y}_1^* - \hat{y}^{\text{ref}}$ is not simply a^2 times the variance of $\hat{y}_1 - \hat{y}^{\text{ref}}$, but is influenced by the distribution of the reference itself. Thus, only when $a = 1$, the variance of $\hat{y}_1^* - \hat{y}^{\text{ref}}$ exactly matches that of $\hat{y}_1 - \hat{y}^{\text{ref}}$. If $a = -1$, while the spread of \hat{y}_1^* remains unchanged from that of \hat{y}_1 , the spread of the errors of \hat{y}_1^* will increase. For general values of a , it is possible that fortuitously, the variance of prediction errors decreases after scaling.

Practical Considerations: In the above discussion, we designated the predictor with low MSE as an internal reference, \hat{y}_2 , interpreting it as the lower-bias model. However, this predictor will also have a low MAD only if all errors, $\hat{y}_2 - \hat{y}^{\text{ref}}$, have the same sign. In particular, if all errors are negative, then $\text{MAD} = -\text{MSE}$. In practice, a vanishing MSE for an approximate model often suggests a multimodal error distribution centered around zero, where positive and negative errors cancel each other out. In such cases, MSE can significantly underestimate the actual bias, making it an unreliable metric. A more robust measure of bias is MAD, which accounts for the magnitude of errors irrespective of sign. Thus, in this study, we select \hat{y}_2 as the predictor with the smallest MAD instead of the smallest MSE. This change does not affect any of the derivations presented above. Notably, the MSE of the scaled low-variance predictor, \hat{y}_1^* , remains close to that of \hat{y}_2 , ensuring bias correction. Furthermore, since the variance of \hat{y}_1^* remains approximately the same as that of \hat{y}_1 (for $a \approx 1$) the spread of errors is expected to be narrower. As a result, the MAD of \hat{y}_1^* will typically be smaller than that of \hat{y}_2 , reflecting a better balance between bias and variance.

4 Results and Discussions

4.1 Overall trends across methods

Figure 2 presents an overview of the performance of various theoretical methods using the TBE of STGs from Ref. [14] as a reference. For consistency, all results are reported with the aug-cc-pVDZ basis set; results for other basis sets are provided in the Supplementary Information (SI). CC3 results are taken from Ref. [14]. Detailed error metrics for the wavefunction methods are provided in Table 1. For all methods listed in Table 1, increasing the basis set to aug-cc-pVTZ yields only minimal improvement. The reference (*i.e.*, TBE) S_1 energies were computed at the CC3/aug-cc-pVTZ level with a post-CC3 correction via EOM-CCSDT (using the 6-31+G(d) basis set), while the T_1 energies were obtained at the EOM-CCSD/aug-cc-pVTZ level with a post-CCSD correction via CC3 using the aug-cc-pVDZ basis set [14]. Although the TBE approach treats S_1 and T_1 energies using different protocols, both are estimated at higher levels of theory currently available.

Among all methods, CC3/aug-cc-pVDZ shows the lowest values for MSE, MAD, and SDE (-1 , 10 , and 13 meV (milli-eV), respectively; see Table 1). When combined with the aug-cc-pVTZ basis set, CC3 essentially reproduces the TBE results. The next best performance is observed for L-CC2 with an MAD and SDE of 16 and 13 meV. L-ADC(2)/aug-cc-pVTZ results show an MAD and SDE of 22 and 13 meV, respectively, which are similar to the corresponding ADC(2) values of 20 and 16 meV.

Both the mean error and the spread of the error are significant for EOM-CCSD (Figure 2). Its MSE indicates that its predictions can serve as an upper bound for negative STGs; however, an SDE of approximately 80 – 90 meV diminishes confidence in predictions

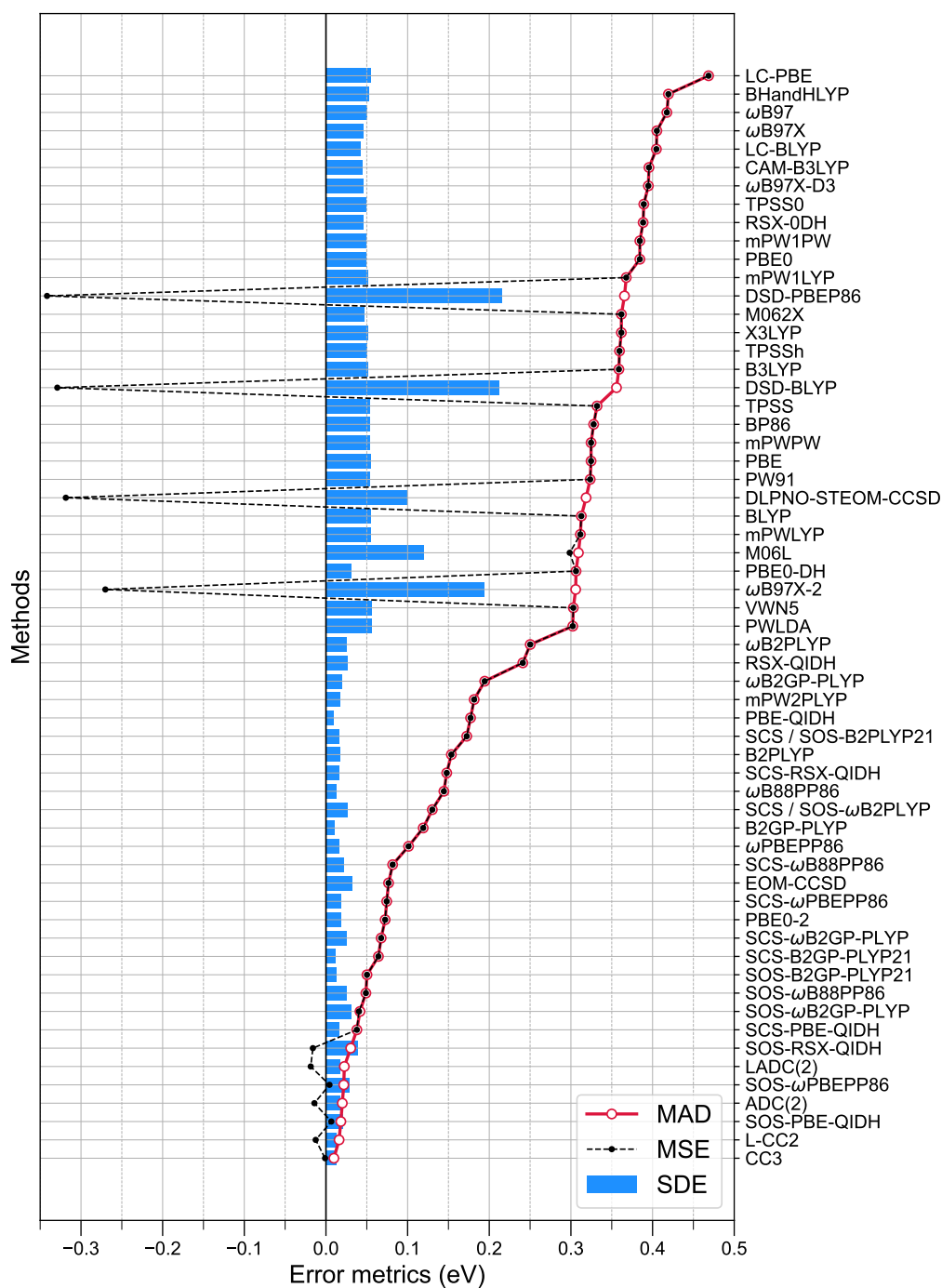


Figure 2: Error metrics for various methods using the aug-cc-pVDZ basis set to predict 12 theoretical best estimates of STGs for triangular molecules. MAD, MSE, and SDE represent mean absolute deviation, mean signed error, and standard deviation, respectively. Methods are ordered by increasing MAD, with a line included as a visual guide. CC3 and EOM-CCSD results are from Ref [14].

of gaps smaller than 0.1 eV, potentially leading to false negatives (*i.e.*, systems with truly negative gaps might be predicted as having positive gaps). The large SDE suggests that the error is not systematic, hence, not all small, positive STGs predicted by EOM-CCSD may be reliably expected to be negative. In particular, the similarity-transformed local variant, DLPNO-STEOM-CCSD, exhibits a bias exceeding 0.25 eV with an SDE around 0.1 eV (see Figure 2), rendering it unsuitable for applications involving negative STG systems [68, 69].

Table 1: Error metrics for predicting twelve values of S_1 & T_1 energies, and STG of triangular molecules. For various methods, values are reported compared to the theoretical best estimates from Ref. [14]. MSE: mean signed error, MAD: mean absolute deviation, SDE: standard deviation of the error, minE: minimal error, and maxE: maximal error. In all cases, the basis set is aug-cc-pVDZ. Wherever necessary, the convention for deviation is ‘Method–TBE.’ All values are in eV.

Method	Energy	MSE	MAD	SDE	minE	maxE
L-CC2/aug-cc-pVDZ ^a	S_1	0.047	0.047	0.016	0.020	0.071
	T_1	0.060	0.060	0.017	0.038	0.091
	STG	-0.013	0.016	0.013	-0.028	0.010
L-CC2/aug-cc-pVTZ ^a	S_1	0.051	0.051	0.010	0.035	0.064
	T_1	0.065	0.065	0.016	0.032	0.090
	STG	-0.014	0.015	0.010	-0.028	0.005
L-ADC(2)/aug-cc-pVDZ ^a	S_1	0.006	0.031	0.035	-0.056	0.056
	T_1	0.025	0.030	0.032	-0.020	0.078
	STG	-0.019	0.023	0.017	-0.038	0.023
L-ADC(2)/aug-cc-pVTZ ^a	S_1	0.003	0.017	0.021	-0.037	0.039
	T_1	0.023	0.023	0.018	-0.002	0.052
	STG	-0.020	0.022	0.013	-0.036	0.009
ADC2/aug-cc-pVTZ ^a	S_1	-0.000	0.021	0.026	-0.051	0.050
	T_1	0.015	0.022	0.022	-0.023	0.049
	STG	-0.016	0.020	0.016	-0.039	0.021
CC3/aug-cc-pVDZ ^b	S_1	0.001	0.015	0.018	-0.030	0.026
	T_1	0.002	0.016	0.020	-0.038	0.037
	STG	-0.001	0.010	0.013	-0.035	0.015

^a This work

^b From Ref. [14]

Among the DFT methods, the dh-DFT approaches B2GP-PLYP and PBE-QIDH display very small SDEs (Figure 2), indicating that their deviations from the TBE values are primarily systematic. The spin-component-scaled (SCS) and opposite-spin-scaled (SOS) variants of these methods exhibit reduced MSE and MAD at the expense of larger SDEs. With few exceptions, the remaining DFAs show large errors, rendering them unreliable for first-principles identification of negative STG systems.

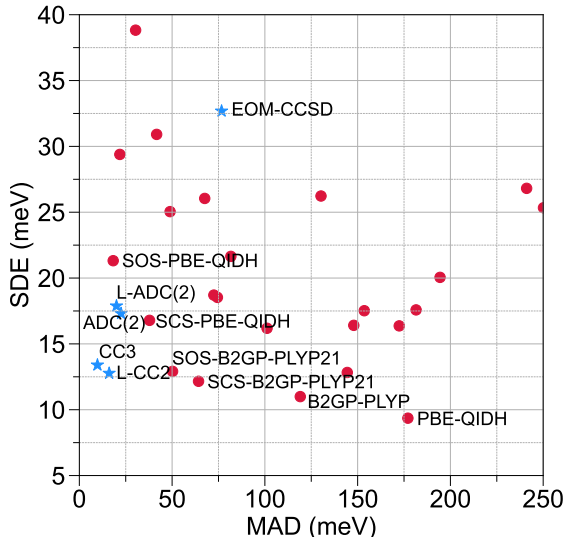


Figure 3: Bias-variance tradeoff in various methods as a scatterplot of MAD versus SDE for predicting 12 theoretical best estimates of STGs in triangular molecules. Wavefunction methods are marked with blue stars, and DFAs with red circles. For clarity, names are shown only for selected points. All results are based on the aug-cc-pVDZ basis set. CC3 and EOM-CCSD results are from Ref [14]

4.2 Bias-variance tradeoff across methods

If the magnitude of negative STGs exceeds 0.2 eV, methods with mean errors ≈ 0.1 eV may still allow for qualitative identification. However, for systems where the STG is below ≈ 0.1 eV, similar prediction errors become too large to yield reliable qualitative conclusions. Figure 2 reveals interesting trends in the bias-variance tradeoff in various methods: while some methods exhibit a high MAD, they maintain a very low SDE. These cases are highlighted in Figure 3, which plots MAD versus SDE for various methods (excluding those with high MAD or SDE). Overall, CC3 and L-CC2 demonstrate superior performance with low MAD and SDE, whereas several DFT approaches—notably, B2GP-PLYP and PBE-QIDH—exhibit remarkably small variance. In particular, PBE-QIDH shows an SDE of less than 10 meV, indicating that its predictions are narrowly clustered around the TBE values but shifted by a constant systematic error. Although the MAD of PBE-QIDH exceeds 175 meV, systematic errors are generally easier to correct through linear regression than the non-systematic errors associated with high variance. For properties such as atomization or formation energies, DFT predictions are often corrected for systematic errors via dressed atom corrections, leading to lower errors for DFAs on the higher rungs of “Jacob’s ladder” [70, 56, 71].

Among the local correlated methods, L-CC2 exhibits MAD and SDE values close to those of CC3, while L-ADC2 shows a slightly larger SDE than L-CC2 (Figure 3). In contrast, the dh-DFT methods B2GP-PLYP and PBE-QIDH display SDEs that are smaller

than L-CC2’s, but their MADs are larger by about an order of magnitude. To explore the potential of low-variance, high-bias methods, we applied a least-squares correction to the STG predictions of B2GP-PLYP, PBE-QIDH, L-ADC(2), and L-CC2 using TBE values as the reference; the results are collected in Table 2. As expected, the MSE becomes zero after linear correction. L-ADC(2) and L-CC2 show MADs of 0.023 and 0.016 eV with SDEs of 0.017 and 0.013 eV, respectively, with only slight improvement upon correction, indicating that their errors are primarily non-systematic. In contrast, dh-DFT methods B2GP-PLYP and PBE-QIDH, which initially exhibit MADs of 0.119 and 0.177 eV and SDEs of 0.011 and 0.009 eV respectively, experience a dramatic drop in MAD (to below 0.01 eV) after correction, while retaining their low SDEs. This implies that the errors in these dh-DFT methods are predominantly systematic. A similar analysis for the SCS and SOS variants of these methods, presented in Table 3, confirms that all fixed dh-DFT methods show reduced MAD and SDE values, indicating that their prediction errors are largely systematic when compared to TBE.

Table 2: For various methods (aug-cc-pVDZ basis set) STGs of benchmark systems (Figure 1) are presented before and after bias-correction. Error metrics and the reference TBE values are also provided. MSE: mean signed error, MAE: mean absolute error, and SDE: standard deviation of the error. Wherever necessary, the convention for deviation is ‘Method–TBE.’ All values are in eV.

#	B2GP-PLYP		PBE-QIDH		L-ADC2		L-CC2		TBE ^e
	corr. ^a		corr. ^b		corr. ^c		corr. ^d		
1	-0.095	-0.220	-0.035	-0.215	-0.255	-0.229	-0.247	-0.229	-0.219
2	-0.007	-0.126	0.037	-0.141	-0.134	-0.116	-0.128	-0.116	-0.131
3	0.020	-0.098	0.081	-0.095	-0.120	-0.103	-0.109	-0.098	-0.101
4	-0.014	-0.134	0.062	-0.115	-0.132	-0.114	-0.130	-0.118	-0.119
5	0.005	-0.114	0.082	-0.094	-0.138	-0.119	-0.127	-0.115	-0.103
6	0.042	-0.074	0.094	-0.082	-0.102	-0.086	-0.086	-0.076	-0.071
7	0.070	-0.044	0.122	-0.053	-0.080	-0.065	-0.069	-0.059	-0.042
8	0.081	-0.033	0.132	-0.043	-0.063	-0.049	-0.052	-0.043	-0.029
9	-0.080	-0.204	-0.017	-0.196	-0.220	-0.197	-0.215	-0.199	-0.199
10	-0.173	-0.303	-0.126	-0.308	-0.318	-0.289	-0.325	-0.304	-0.305
11	-0.049	-0.171	-0.005	-0.184	-0.199	-0.177	-0.187	-0.172	-0.195
12	0.177	0.070	0.246	0.074	0.085	0.090	0.072	0.075	0.062
MSE	0.119	0.000	0.177	0.000	-0.019	0.000	-0.013	0.000	
MAD	0.119	0.007	0.177	0.008	0.023	0.014	0.016	0.010	
SDE	0.011	0.009	0.009	0.009	0.017	0.016	0.013	0.012	

^a Corrected with slope = 1.0654 and intercept = -0.1190

^b Corrected with slope = 1.0284 and intercept = -0.1787

^c Corrected with slope = 0.9409 and intercept = -0.0103

^d Corrected with slope = 0.9546 and intercept = -0.0065

^e From Ref. [14]

Table 3: Error metrics for predicting twelve values of S_1 and T_1 energetics of triangular molecules reported in Ref. [14]. Values are reported compared to the theoretical best estimates (TBE) from Ref. [14]. In all cases, the basis set is aug-cc-pVDZ, and the geometries are from Ref. [14]. MSE: mean signed error, MAE: mean absolute error, and SDE: standard deviation of the error. Wherever necessary, the convention for deviation is ‘Method–TBE.’ All values are in eV.

Method	Energy	Slope	Intercept	Before correction		After correction	
				MAE	SDE	MAE	SDE
B2GP-PLYP	S_1	1.0350	-0.2382	0.184	0.030	0.012	0.020
	T_1	1.0294	-0.1105	0.065	0.031	0.018	0.024
	STG	1.0654	-0.1190	0.119	0.011	0.007	0.009
SOS-B2GP-PLYP21	S_1	1.0164	-0.2574	0.231	0.015	0.008	0.011
	T_1	1.0048	-0.1889	0.181	0.019	0.013	0.018
	STG	0.9167	-0.0561	0.050	0.013	0.007	0.010
SCS-B2GP-PLYP21	S_1	1.0086	-0.2948	0.281	0.013	0.009	0.012
	T_1	1.0000	-0.2164	0.216	0.020	0.015	0.020
	STG	0.9246	-0.0685	0.064	0.012	0.008	0.009
PBE-QIDH	S_1	0.9627	-0.2158	0.277	0.034	0.013	0.023
	T_1	0.9693	-0.0514	0.100	0.033	0.017	0.025
	STG	1.0284	-0.1787	0.177	0.009	0.008	0.009
SOS-PBE-QIDH	S_1	1.0120	-0.1281	0.110	0.012	0.008	0.009
	T_1	0.9889	-0.0862	0.104	0.017	0.012	0.016
	STG	0.8423	-0.0246	0.018	0.021	0.010	0.012
SCS-PBE-QIDH	S_1	1.0091	-0.1479	0.134	0.011	0.007	0.009
	T_1	0.9907	-0.0818	0.096	0.018	0.013	0.017
	STG	0.8815	-0.0477	0.038	0.017	0.009	0.011

4.3 Internally referenced bias-variance correction for double-hybrid DFT

While one can use L-CC2, CC3, or TBE values to correct PBE-QIDH predictions through linear scaling, we further investigated whether the low-variance DFT methods—B2GP-PLYP and PBE-QIDH—can be adjusted to minimize bias. The PBE-QIDH DFA is defined as follows [59]:

$$E_{xc}^{\text{PBE-QIDH}}[\rho] = a_x E_x^{\text{HF}} + (1 - a_x) E_x^{\text{PBE}} + a_c E_c^{\text{MP2}} + (1 - a_c) E_c^{\text{PBE}}. \quad (4.1)$$

Here, the coefficients a_x and a_c control the fraction of exact exchange (via Hartree-Fock) and MP2-level correlation, respectively. In the standard formulation, PBE-QIDH ($a_x = 0.69$ and $a_c = 0.33$) [72] belongs to a family of dh-DFAs with $a_c = a_x^3$ delivering low errors for STG [73]. Similarly, B2GP-PLYP is based on the GGA-B88 exchange functional and a combination of LYP-GGA and VWN3-LDA correlation functionals:

$$E_{xc}^{\text{B2GP-PLYP}}[\rho] = a_x E_x^{\text{HF}} + (1 - a_x) E_x^{\text{B88}} + a_c E_c^{\text{MP2}} + (1 - a_c) (E_c^{\text{VWN3}} + E_c^{\text{LYP}}) \quad (4.2)$$

with standard mixing coefficients $a_x = 0.65$ and $a_c = 0.36$ [74, 75, 76].

Prior studies have shown that the a_x - a_c parameter space of B2GP-PLYP exhibits a continuous range of optimal parameters depending on the target property [58, 23]. For instance, Tarnopolsky *et al.* demonstrated variations in the SDE for thermochemistry and reaction barriers as a function of a_x and a_c , and proposed the B2T-PLYP and B2K-PLYP dh-DFAs with $(a_x = 0.60, a_c = 0.31)$ and $(a_x = 0.72, a_c = 0.40)$, respectively [22]. However, while these studies focused on a single error metric across different properties—emphasizing variance because bias in thermochemistry is corrected through quasi-atomic corrections[70, 56, 71]—the bias-variance trade-off for a single property such as the STG has not been thoroughly examined.

Using B2GP-PLYP and PBE-QIDH DFAs, we scanned a_x and a_c , and computed error metrics for all 12 benchmark STGs using TBE as the reference. As shown in Figure 4, both dh-DFAs exhibit low SDEs for the default mixing parameters, and a continuous range of (a_x, a_c) combinations yielding zero MSE is observed (Figure 4, top panels). Some calculations failed to converge when a_x and $a_c \approx 0$; these are not shown in Figure 4. However, the minimum MAD is achieved at $a_x = 0.75$ and $a_c = 0.55$, with both DFAs delivering MADs of approximately 25 meV compared to TBE. We denote these optimized parameterizations as B2GP-PLYP (75,55) and PBE-QIDH (75,55). To assess the variation of optimal a_x and a_c across error metrics for S_1 and T_1 energies separately, we performed a comparative analysis (Table S1) using PBE-QIDH. Notably, increased accuracy in S_1 energies is observed when both mixing parameters approach 1 (with $a_x = 0.90$ and $a_c = 0.85$ yielding a MAD of 68 meV), while the lowest MAD for T_1 (22 meV) is obtained for $a_x = 0.5$ and $a_c = 0.15$.

To apply the scaling protocol discussed in Section 3, the default B2GP-PLYP and PBE-QIDH parameterizations serve as the low-variance estimators (y_1 in Eq.(3.1)), while the (75,55) variants, which exhibit the lowest MAD, serve as the reference low-bias estimators (y_2 in Eq.(3.1)). We then determine the slope and intercept via linear regression to correct the bias, with the corrected predictions denoted as B2GP-PLYP* and PBE-QIDH*. Table 4 presents the STG values for the 12 benchmark systems predicted by the bias-corrected dh-DFAs. Importantly, the scaling procedure does not require any additional high-level reference data to identify the low-bias or low-variance domain in the parameter space of dh-DFAs. The bias-corrected predictions, which simultaneously reflect the small SDE of the base dh-DFAs and the low MAD of the internal references, achieve MAD|SDE values of 10|12 and 9|11 meV for B2GP-PLYP* and PBE-QIDH*, respectively, with respect to TBE.

The overall correlation between the predicted values and TBE is illustrated in Figure 5. Due to the large bias in the original dh-DFT predictions, the Pearson correlation coefficients are strongly negative ($\rho = -0.61$ for B2GP-PLYP and $\rho = -2.45$ for PBE-QIDH; see Figure 5a). Upon applying the internally referenced scaling, the correlation improves markedly to $\rho = 0.98$ for both DFAs, with all 12 values aligning with TBE more closely than those from L-ADC(2), L-CC2, or even CC3. The overall performance of the

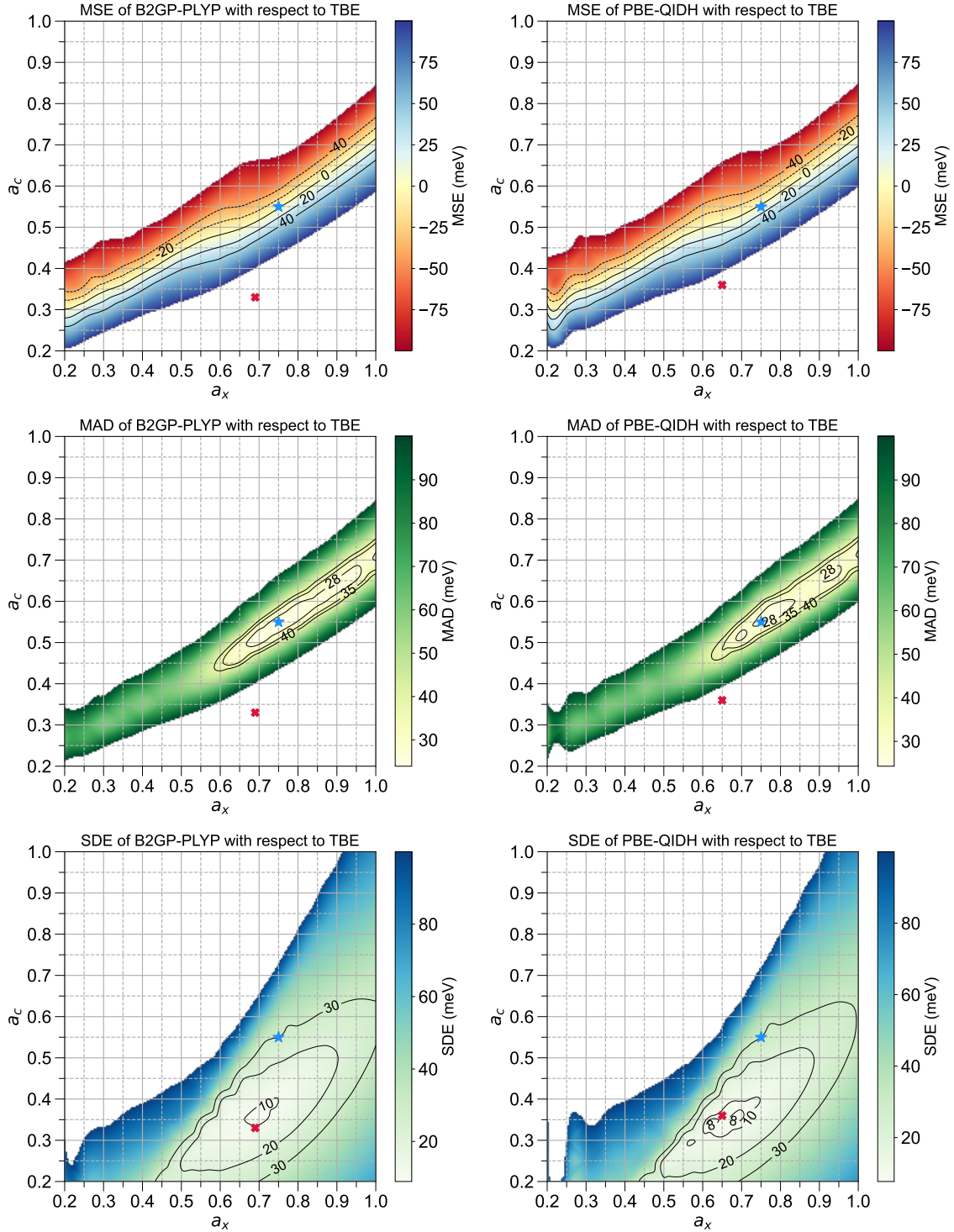


Figure 4: Dependence of prediction errors of dh-DFT with exchange and correlation mixing parameters a_x and a_c (See Eq. 4.1 and Eq. 4.2). MSE, MAD and SDE (in meV) are shown for B2GP-PLYP (left panels) and PBE-QIDH (right panels) compared to TBE. Values of a_x and a_c were sampled in steps of 0.05 and the surfaces were smoothed using cubic functions. In all plots, the default mixing coefficients are marked by a red cross—(0.65, 0.36) for B2GP-PLYP and (0.69, 0.33) for PBE-QIDH—and coefficients that minimize MAD are marked by a blue star—(0.75, 0.55) for both B2GP-PLYP and PBE-QIDH.

Table 4: STGs of benchmark systems shown in Figure 1 calculated with double-hybrid DFT methods using the aug-cc-pVDZ basis set. The error metrics MSE (mean signed error), MAD (mean absolute deviation), and SDE (standard deviation of the error) are with respect to theoretical best estimates given in Table 2. All values are in eV.

#	B2GP-PLYP			PBE-QIDH		
	(65, 36)	(75, 55)	scaled ^a	(69, 33)	(75, 55)	scaled ^b
1	-0.095	-0.245	-0.231	-0.035	-0.239	-0.216
2	-0.007	-0.102	-0.130	0.037	-0.094	-0.138
3	0.020	-0.104	-0.099	0.081	-0.096	-0.089
4	-0.014	-0.178	-0.138	0.062	-0.170	-0.110
5	0.005	-0.153	-0.116	0.082	-0.144	-0.088
6	0.042	-0.064	-0.074	0.094	-0.056	-0.075
7	0.070	-0.034	-0.041	0.122	-0.024	-0.045
8	0.081	-0.016	-0.029	0.132	-0.007	-0.034
9	-0.080	-0.227	-0.214	-0.017	-0.222	-0.197
10	-0.173	-0.299	-0.321	-0.126	-0.295	-0.316
11	-0.049	-0.154	-0.178	-0.005	-0.148	-0.183
12	0.177	0.086	0.082	0.246	0.095	0.091
MSE	0.119	-0.003	-0.003	0.177	0.004	0.004
MAD	0.119	0.025	0.010	0.177	0.027	0.009
SDE	0.011	0.030	0.012	0.009	0.030	0.011

^a Calculated by scaling B2GP-PLYP (65,36) values using slope = 1.1521 and intercept=-0.1220

^b Calculated by scaling PBE-QIDH (69,33) values using slope = 1.0940 and intercept=-0.1780

scaling procedure stems from the exceptionally small variance of the dh-DFAs and the low MAD achieved with the (75,55) parameterizations.

4.4 Application to heptazine derivatives

To probe the applicability of our bias-correction strategy, we focused on four DFIST candidates proposed in Ref. [4]. At the T_1 geometry, the STGs of HzTFEX₂, HzPipX₂, HzTFEP₂, and HzTFET₂ at the EOM-CCSD, ADC(2), L-CC2, and SCS-ADC(2) levels exhibit smaller magnitudes[4] than those of the twelve triangular systems discussed above. This difference is attributed to the change in geometry, as STGs generally increase when moving away from the ground state minimum (S_0) as pointed out from the context of excited-state nuclear dynamics[77] and the pseudo-Jahn–Teller effect [25]. Despite the larger molecular size of the heptazine derivatives compared to the triangular systems, local methods such as L-ADC(2) and L-CC2 provide significant speedups over their canonical counterparts, while dh-DFT calculations remain computationally feasible.

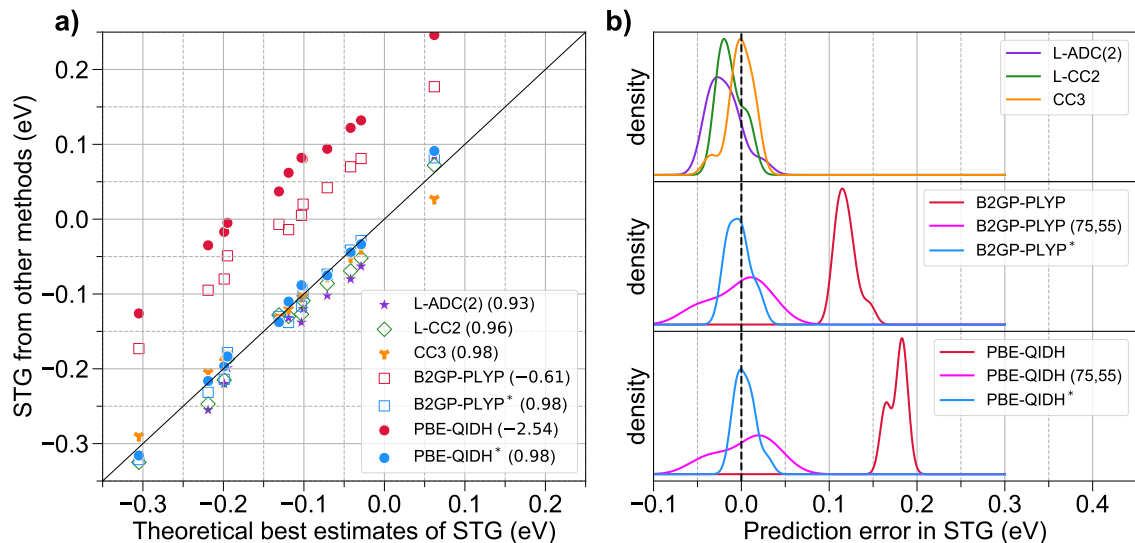


Figure 5: Comparison of 12 STGs of benchmark systems across methods: a) Scatterplot of values predicted by various methods (with the aug-cc-pVDZ basis set) versus theoretical best estimates (TBE). TBE and CC3 results are from Ref. [14]. b) Distribution of errors in predicted STGs relative to TBE shown as smooth densities.

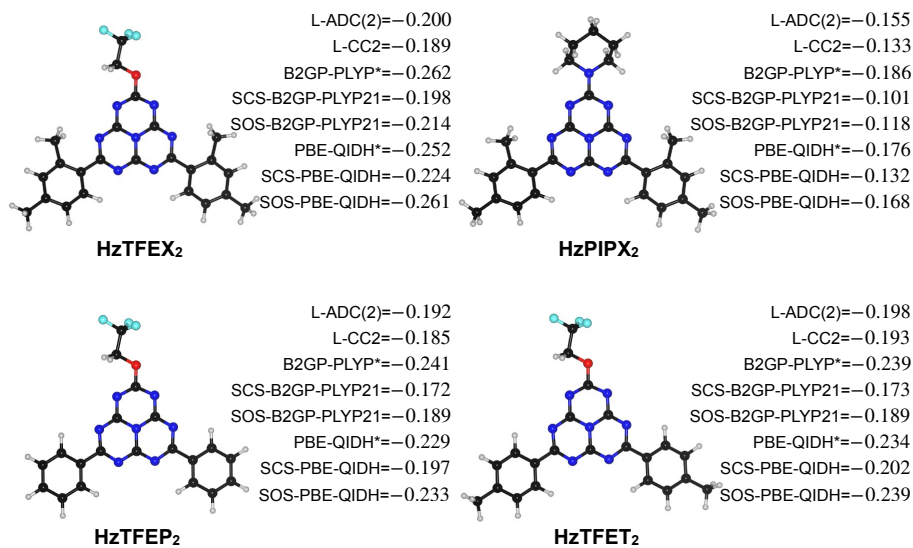


Figure 6: Heptazine derivatives proposed as candidates for light emitters exhibiting delayed fluorescence from inverted singlet and triplet excited states (DFIST) in Ref. [4] are shown along with their computed STG values (in eV) from various methods. B2GP-PLYP* and PBE-QIDH* indicate that the results of the base methods B2GP-PLYP and PBE-QIDH are corrected with respect to their variants with $a_x = 0.75$ and $a_c = 0.55$; more details are available in the SI. Atoms in white|black|blue|red|cyan are H|C|N|O|F.

For all four systems, geometry optimization was performed at the ω B97X-D3/def2TZVP

level (see SI for details), followed by single-point excited-state energy calculations. The STGs of these four systems, obtained from various methods, are presented in Figure 6. In the absence of a high-fidelity reference such as TBE for these systems, L-CC2 results are considered the most reliable. We used B2GP-PLYP (75,55) energies as references to scale the predictions from B2GP-PLYP (65,36) and similarly corrected PBE-QIDH (69,33) predictions using the (75,55) configuration. Notably, the application of the internal scaling does not require any additional high-level reference to identify the low-bias or low-variance domain in the parameter space of dh-DFAs. This enables a straightforward application of our internally referenced scaling procedure, which corrects systematic errors without requiring external high-level reference data.

Among the results from various dh-DFAs, SCS-PBE-QIDH shows the best agreement with L-CC2, achieving an MAD of 0.014 eV. In contrast, bias-corrected results for B2GP-PLYP and PBE-QIDH are systematically more negative than the L-CC2 values, with MADs of 0.057 eV and 0.048 eV, respectively. While one might argue that simply shifting the results of these two DFAs could render the STGs negative, our correction is performed without requiring reference values from another method. As in the case of triangular benchmark systems (shown in Figure 1), B2GP-PLYP exhibits a smaller bias compared to PBE-QIDH. Furthermore, for triangular systems, we observed that L-CC2’s error relative to the TBE is consistently shifted by -0.013 eV, whereas the errors of the (75,55) variant of the two dh-DFAs are centered around zero (albeit with a large spread), as shown in Figure 5. Consequently, compared to L-CC2, the bias-corrected dh-DFAs are expected to exhibit a non-vanishing MSE; indeed, the MSE values for B2GP-PLYP (75,55) and PBE-QIDH (75,55) are -0.057 eV and -0.048 eV, respectively. Compared to a more accurate reference such as CC3 (which is practically challenging for the four heptazine derivatives), our bias-corrected results may show better agreement than the other methods discussed. Moreover, it is possible to identify combinations of a_x and a_c that yield low bias and low variance relative to L-CC2, which can be further explored for extending the bias correction scheme to larger datasets lacking high-level reference data.

5 Conclusions

First principles excited state modeling plays a crucial role in the identification of new molecular light emitters with a negative S_1 - T_1 energy gap. Historically, theoretical interest in such molecules existed for a long time in the context of Hund’s rule violation[78, 79, 80, 81, 82]. Yet, revived interest in them increased since their identification through first principles modeling[83, 84]. Although individual S_1 and T_1 energies are challenging to predict with high precision, the error cancellation inherent in STG calculations allows for improved accuracy, even when the reported gaps are less than 0.1 eV. Benchmarking twelve STG energy gaps in triangular molecules, we find that local wavefunction methods—specifically L-CC2 and L-ADC2—deliver mean errors of approximately 15 meV with correspondingly low standard deviations, providing both exceptional accuracy and

the computational speed required for high-throughput screening of medium size molecules such as azaphenalenenes with bulky substitutions.

In parallel, we show that double-hybrid DFT approximations—though initially marked by high systematic errors—can be significantly improved through linear regression-based bias correction without depending on a high-level reference. For example, the PBE-QIDH method in its default configuration (69% exact exchange and 33% MP2-level correlation) exhibits an impressively low variance (9 meV) but high mean errors; by adjusting the parameters to 75% exchange and 55% correlation, the mean error is reduced to 4 meV, albeit with increased variance. We propose a bias correction strategy to leverage the bias-variance tradeoff intrinsic the dh-DFA formalisms. Using a suitable low-bias method as an internal reference, the approach corrects systematic errors in low-variance models, thereby enabling quantitatively reliable negative STG estimations. In the case of four heptazine derivatives, the SCS and SOS variants of both B2GP-PLYP and PBE-QIDH—though not subjected to bias correction—yield STG predictions in better agreement with L-CC2, suggesting that these variants naturally mitigate some of the bias in standard dh-DFT. However, bias correction remains valuable for further refining low-variance models, particularly when an appropriate low-bias reference is available.

The purpose of this study is not to advocate different models for different properties but to leverage the intrinsic bias-variance tradeoff for accurate STG predictions. Open questions remain regarding the performance of these parameterized models for positive STGs and systems with charge-transfer excitations[85]. Robust application of our strategy requires reliable reference datasets and could benefit from further bias-variance analysis using alternative information-based metrics [86]. Overall, the findings of this study establish a mathematically sound framework for predictive modeling in first-principles molecular design, with promising implications for the development of novel light emitters and other applications.

6 Supplementary Information

i) Dataset of S_1 , T_1 and S_1 - T_1 energies of twelve triangular molecules calculated with various methods and basis sets. ii) Figures S1–S3 present error metrics for cc-pVDZ, cc-pVTZ, and aug-cc-pVTZ basis sets; iii) Tables S1 presents optimal a_x and a_c along with the associated error metrics for different energies; iv) Tables S2–S3 present excited state energies of heptazine derivatives; v) Equilibrium coordinates of heptazine derivatives.

7 Data Availability

The data that support the findings of this study are within the article and its supplementary material.

8 Acknowledgments

We thank Prof. Denis Jacquemin for commenting on the ADC(2) and CC2 results of the benchmark triangular molecules. We acknowledge the support of the Department of Atomic Energy, Government of India, under Project Identification No. RTI 4007. All calculations have been performed using the Helios computer cluster, which is an integral part of the MolDis Big Data facility, TIFR Hyderabad (<http://moldis.tifrh.res.in>).

9 Author Declarations

9.1 Author contributions

AM: Conceptualization (equal); Analysis (equal); Data collection (equal); Writing (equal).
RR: Conceptualization (equal); Analysis (equal); Data collection (equal); Funding acquisition; Project administration and supervision; Resources; Writing (equal).

9.2 Conflicts of Interest

The authors have no conflicts of interest to disclose.

References

- [1] Hiroki Uoyama, Kenichi Goushi, Katsuyuki Shizu, Hiroko Nomura, and Chihaya Adachi. Highly efficient organic light-emitting diodes from delayed fluorescence. *Nature*, 492(7428):234–238, 2012. URL <https://doi.org/10.1038/nature11687>.
- [2] John Marques Dos Santos, David Hall, Biju Basumatary, Megan Bryden, Dongyang Chen, Praveen Choudhary, Thomas Comerford, Ettore Crovini, Andrew Danos, Joydip De, et al. The golden age of thermally activated delayed fluorescence materials: design and exploitation. *Chem. Rev.*, page 4322, 2024. URL <https://doi.org/10.1021/acs.chemrev.3c00755>.
- [3] Xian-Kai Chen, Dongwook Kim, and Jean-Luc Brédas. Thermally activated delayed fluorescence (TADF) path toward efficient electroluminescence in purely organic materials: molecular level insight. *Acc. Chem. Res.*, 51(9):2215–2224, 2018. URL <https://doi.org/10.1021/acs.accounts.8b00174>.
- [4] Naoya Aizawa, Yong-Jin Pu, Yu Harabuchi, Atsuko Nihonyanagi, Ryotaro Ibuka, Hiroyuki Inuzuka, Barun Dhara, Yuki Koyama, Ken-ichi Nakayama, Satoshi Maeda, et al. Delayed fluorescence from inverted singlet and triplet excited states. *Nature*, 609(7927):502–506, 2022. URL <https://doi.org/10.1038/s41586-022-05132-y>.

- [5] Kenneth D Wilson, William H Styers, Samuel A Wood, R Claude Woods, Robert J McMahon, Zhe Liu, Yang Yang, and Etienne Garand. Spectroscopic Quantification of the Inverted Singlet–Triplet Gap in Pentaazaphenalene. *J. Am. Chem. Soc.*, 146(23):15688–15692, 2024. URL <https://doi.org/10.1021/jacs.4c05043>.
- [6] Yu Kusakabe, Katsuyuki Shizu, Hiroyuki Tanaka, Kazuo Tanaka, and Hironori Kaji. An inverted singlet-triplet excited state in a pentaazaphenalene derivative (5AP-N (C12) 2). *Appl. Phys. Express*, 17(6):061001, 2024. URL <https://doi.org/10.35848/1882-0786/ad4e96>.
- [7] Taehyun Won, Ken-ichi Nakayama, and Naoya Aizawa. Inverted singlet–triplet emitters for organic light-emitting diodes. *Chem. Phys. Rev.*, 4(2), 2023. URL <https://doi.org/10.1063/5.0152834>.
- [8] Jie Li, Zhi Li, Hui Liu, Heqi Gong, Jincheng Zhang, Yali Yao, and Qiang Guo. Organic molecules with inverted singlet-triplet gaps. *Front. Chem.*, 10:999856, 2022. URL <https://doi.org/10.3389/fchem.2022.999856>.
- [9] Lucie Tučková, Michal Straka, Rashid R Valiev, and Dage Sundholm. On the origin of the inverted singlet–triplet gap of the 5th generation light-emitting molecules. *Phys. Chem. Chem. Phys.*, 24(31):18713–18721, 2022. URL <https://doi.org/10.1039/D2CP02364D>.
- [10] Andreas Dreuw and Marvin Hoffmann. The inverted singlet–triplet gap: a vanishing myth? *Front. Chem.*, 11, 2023. URL <https://doi.org/10.3389/fchem.2023.1239604>.
- [11] Soumen Ghosh and Kalishankar Bhattacharyya. Origin of the failure of density functional theories in predicting inverted singlet–triplet gaps. *J. Phys. Chem. A*, 126(8):1378–1385, 2022. URL <https://doi.org/10.1021/acs.jpca.1c10492>.
- [12] Gaetano Ricci, Emilio San-Fabián, Yoann Olivier, and Juan-Carlos Sancho-García. Singlet-triplet excited-state inversion in heptazine and related molecules: assessment of TD-DFT and ab initio methods. *ChemPhysChem*, 22(6):553–560, 2021. URL <http://doi.org/10.1002/cphc.202000926>.
- [13] Juan Carlos Sancho-Garcia, Eric Bremond, Gaetano Ricci, AJ Pérez-Jiménez, Yoann Olivier, and Carlo Adamo. Violation of Hund’s rule in molecules: Predicting the excited-state energy inversion by TD-DFT with double-hybrid methods. *J. Chem. Phys.*, 156(3), 2022. URL <https://doi.org/10.1063/5.0076545>.
- [14] Pierre-François Loos, Filippo Lipparini, and Denis Jacquemin. Heptazine, Cyclazine, and Related Compounds: Chemically-Accurate Estimates of the Inverted Singlet–Triplet Gap. *J. Phys. Chem. Lett.*, 14:11069–11075, 2023. URL <https://doi.org/10.1021/acs.jpcllett.3c03042>.

- [15] Marc H Garner, J Terence Blaskovits, and Clémence Corminboeuf. Double-bond delocalization in non-alternant hydrocarbons induces inverted singlet–triplet gaps. *Chem. Sci.*, 14(38):10458–10466, 2023. URL <https://doi.org/10.1039/D3SC03409G>.
- [16] J Terence Blaskovits, Marc H Garner, and Clémence Corminboeuf. Symmetry-Induced Singlet-Triplet Inversions in Non-Alternant Hydrocarbons. *Angew. Chem. Int. Ed.*, 62(15):e202218156, 2023. URL <https://doi.org/10.1002/anie.202218156>.
- [17] Marc H Garner, J Terence Blaskovits, and Clémence Corminboeuf. Enhanced inverted singlet–triplet gaps in azaphenalenenes and non-alternant hydrocarbons. *Chem. Commun.*, 60(15):2070–2073, 2024. URL <https://doi.org/10.1039/D3CC05747J>.
- [18] J Terence Blaskovits, Clémence Corminboeuf, and Marc H Garner. Excited-State Hund’s Rule Violations in Bridged [10]-and [14] Annulene Perimeters. *J. Phys. Chem. A*, 2024. URL <https://doi.org/10.1021/acs.jpca.4c06726>.
- [19] AkshatKumar Nigam, Robert Pollice, Pascal Friederich, and Alán Aspuru-Guzik. Artificial design of organic emitters via a genetic algorithm enhanced by a deep neural network. *Chem. Sci.*, 15(7):2618–2639, 2024. URL <https://doi.org/10.1039/D3SC05306G>.
- [20] J Terence Blaskovits, Clémence Corminboeuf, and Marc H Garner. Singlet–Triplet Inversions in Through-Bond Charge-Transfer States. *J. Phys. Chem. Lett.*, 15(40):10062–10067, 2024. URL <https://doi.org/10.1021/acs.jpcllett.4c02317>.
- [21] Atreyee Majumdar and Raghunathan Ramakrishnan. Resilience of Hund’s rule in the chemical space of small organic molecules. *Phys. Chem. Chem. Phys.*, 26(20):14505–14513, 2024. URL <https://doi.org/10.1039/D4CP00886C>.
- [22] Alex Tarnopolsky, Amir Karton, Rotem Sertchook, Dana Vuzman, and Jan ML Martin. Double-hybrid functionals for thermochemical kinetics. *J. Phys. Chem. A*, 112(1):3–8, 2008. URL <https://doi.org/10.1021/jp710179r>.
- [23] Lars Goerigk and Stefan Grimme. Efficient and Accurate Double-Hybrid-Meta-GGA Density Functionals: Evaluation with the Extended GMTKN30 Database for General Main Group Thermochemistry, Kinetics, and Noncovalent Interactions. *J. Chem. Theory Comput.*, 7(2):291–309, 2011. URL <https://doi.org/10.1021/ct100466k>.
- [24] Lars Goerigk and Stefan Grimme. Double-hybrid density functionals. *Wiley Interdiscip. Rev. Comput. Mol. Sci.*, 4(6):576–600, 2014. URL <https://doi.org/10.1002/wcms.1193>.
- [25] Atreyee Majumdar, Komal Jindal, Surajit Das, and Raghunathan Ramakrishnan. Influence of pseudo-Jahn–Teller activity on the singlet–triplet gap of azaphenalenenes.

- Phys. Chem. Chem. Phys.*, 26(42):26723–26733, 2024. URL <https://doi.org/10.1039/D4CP02761B>.
- [26] Katrin Freundorfer, Daniel Kats, Tatiana Korona, and Martin Schütz. Local CC2 response method for triplet states based on Laplace transform: Excitation energies and first-order properties. *J. Chem. Phys.*, 133(24), 2010. URL <https://doi.org/10.1063/1.3506684>.
- [27] Martin Schütz. Oscillator strengths, first-order properties, and nuclear gradients for local ADC (2). *J. Chem. Phys.*, 142(21), 2015. URL <https://doi.org/10.1063/1.4921839>.
- [28] HJ Werner, PJ Knowles, G Knizia, FR Manby, M Schütz, P Celani, W Györffy, D Kats, T Korona, R Lindh, et al. MOLPRO, Version 2015.1, A package of ab initio programs, 2015. URL <https://www.molpro.net/>.
- [29] Danylo Kats, Tatiana Korona, and Martin Schütz. Local CC2 electronic excitation energies for large molecules with density fitting. *J. Chem. Phys.*, 125(10), 2006. URL <https://doi.org/10.1063/1.2339021>.
- [30] Milica Feldt and Alex Brown. Assessment of local coupled cluster methods for excited states of BODIPY/Aza-BODIPY families. *J. Comput. Chem.*, 42(3):144–155, 2021. URL <https://doi.org/10.1002/jcc.26442>.
- [31] Mohammad R Momeni and Alex Brown. A local CC2 and TDA-DFT double hybrid study on BODIPY/aza-BODIPY dimers as heavy atom free triplet photosensitizers for photodynamic therapy applications. *J. Phys. Chem. A*, 120(16):2550–2560, 2016. URL <https://doi.org/10.1021/acs.jpca.6b02883>.
- [32] O Vahtras, J Almlöf, and MW Feyereisen. Integral approximations for LCAO-SCF calculations. *Chem. Phys. Lett.*, 213(5-6):514–518, 1993. doi: 10.1016/0009-2614(93)89151-7. URL [https://doi.org/10.1016/0009-2614\(93\)89151-7](https://doi.org/10.1016/0009-2614(93)89151-7).
- [33] Rick A Kendall and Herbert A Früchtl. The impact of the resolution of the identity approximate integral method on modern ab initio algorithm development. *Theor. Chim. Acta*, 97(1):158–163, 1997. URL <https://link.springer.com/article/10.1007/s002140050249>.
- [34] Anna I Krylov and Peter MW Gill. Q-Chem: an engine for innovation. *Wiley Interdiscip. Rev. Comput. Mol. Sci.*, 3(3):317–326, 2013. URL <https://doi.org/10.1002/wcms.1122>.
- [35] Tonatiuh Rangel, Samia M Hamed, Fabien Bruneval, and Jeffrey B Neaton. An assessment of low-lying excitation energies and triplet instabilities of organic molecules with an ab initio Bethe-Salpeter equation approach and the Tamm-Dancoff approximation. *J. Chem. Phys.*, 146(19), 2017. URL <https://doi.org/10.1063/1.4983126>.

- [36] Kalishankar Bhattacharyya. Can TDDFT render the electronic excited states ordering of Azine derivative? A closer investigation with DLPNO-STEOM-CCSD. *Chem. Phys. Lett.*, 779:138827, 2021. URL <https://doi.org/10.1016/j.cplett.2021.138827>.
- [37] Kevin Curtis, Olajumoke Adeyiga, Olabisi Suleiman, and Samuel O Odoh. Building on the strengths of a double-hybrid density functional for excitation energies and inverted singlet-triplet energy gaps. *J. Chem. Phys.*, 158(2), 2023. URL <https://doi.org/10.1063/5.0133727>.
- [38] Lukas Kunze, Thomas Froitzheim, Andreas Hansen, Stefan Grimme, and Jan-Michael Mewes. Δ DFT predicts inverted singlet-triplet gaps with chemical accuracy at a fraction of the cost of wave function-based approaches. *J. Phys. Chem. Lett.*, 15(31):8065–8077, 2024. URL <https://doi.org/10.1021/acs.jpcclett.4c01649>.
- [39] John P Perdew and Karla Schmidt. Jacob’s ladder of density functional approximations for the exchange-correlation energy. In *AIP Conf. Proc.*, volume 577, pages 1–20. American Institute of Physics, 2001. URL <https://doi.org/10.1063/1.1390175>.
- [40] L Wilk, M Nusair, and SH Vosko. The Fermi contact contribution to the Knight shift in Be from self-consistent spin-polarized calculations. *Can. J. Phys.*, 59(4):585–595, 1981. URL <https://doi.org/10.1139/p81-076>.
- [41] John P Perdew and Yue Wang. Accurate and simple analytic representation of the electron-gas correlation energy. *Phys. Rev. B*, 45(23):13244, 1992. URL <https://doi.org/10.1103/PhysRevB.45.13244>.
- [42] Kieron Burke, John P Perdew, and Yue Wang. Derivation of a generalized gradient approximation: The PW91 density functional. In *Electronic Density Functional Theory: recent progress and new directions*, pages 81–111. Springer, 1998. URL https://doi.org/10.1007/978-1-4899-0316-7_7.
- [43] John P Perdew, Kieron Burke, and Matthias Ernzerhof. Generalized gradient approximation made simple. *Phys. Rev. Lett.*, 77(18):3865, 1996. URL <https://doi.org/10.1103/PhysRevLett.77.3865>.
- [44] Philip J Stephens, Frank J Devlin, Cary F Chabalowski, and Michael J Frisch. Ab initio calculation of vibrational absorption and circular dichroism spectra using density functional force fields. *J. Chem. Phys.*, 98(45):11623–11627, 1994. URL <https://doi.org/10.1021/j100096a001>.
- [45] Carlo Adamo and Vincenzo Barone. Toward reliable density functional methods without adjustable parameters: The PBE0 model. *J. Chem. Phys.*, 110(13):6158–6170, 1999. URL <https://doi.org/10.1063/1.478522>.

- [46] Julius T Su, Xin Xu, and William A Goddard. Accurate energies and structures for large water clusters using the X3LYP hybrid density functional. *J. Phys. Chem. A*, 108(47):10518–10526, 2004. URL <https://doi.org/10.1021/jp047502+>.
- [47] Axel D Becke. A new mixing of Hartree–Fock and local density-functional theories. *J. Chem. Phys.*, 98(2):1372–1377, 1993. URL <https://doi.org/10.1063/1.464304>.
- [48] John P Perdew, Adrienn Ruzsinszky, Gábor I Csonka, Lucian A Constantin, and Jianwei Sun. Workhorse semilocal density functional for condensed matter physics and quantum chemistry. *Phys. Rev. Lett.*, 103(2):026403, 2009. URL <http://dx.doi.org/10.1103/PhysRevLett.103.026403>.
- [49] Yan Zhao and Donald G Truhlar. A new local density functional for main-group thermochemistry, transition metal bonding, thermochemical kinetics, and noncovalent interactions. *J. Chem. Phys.*, 125(19), 2006. URL <https://doi.org/10.1063/1.2370993>.
- [50] Yan Zhao and Donald G Truhlar. The M06 suite of density functionals for main group thermochemistry, thermochemical kinetics, noncovalent interactions, excited states, and transition elements: two new functionals and systematic testing of four M06-class functionals and 12 other functionals. *Theor. Chem. Acc.*, 120:215–241, 2008. URL <https://doi.org/10.1007/s00214-007-0310-x>.
- [51] Jeng-Da Chai and Martin Head-Gordon. Systematic optimization of long-range corrected hybrid density functionals. *J. Chem. Phys.*, 128(8), 2008. URL <https://doi.org/10.1063/1.2834918>.
- [52] Takeshi Yanai, David P Tew, and Nicholas C Handy. A new hybrid exchange–correlation functional using the Coulomb-attenuating method (CAM-B3LYP). *J. Phys. Chem. Lett.*, 393(1-3):51–57, 2004. URL <https://doi.org/10.1016/j.cplett.2004.06.011>.
- [53] Yoshihiro Tawada, Takao Tsuneda, Susumu Yanagisawa, Takeshi Yanai, and Kimihiko Hirao. A long-range-corrected time-dependent density functional theory. *J. Chem. Phys.*, 120(18):8425–8433, 2004. URL <https://doi.org/10.1063/1.1688752>.
- [54] Hisayoshi Iikura, Takao Tsuneda, Takeshi Yanai, and Kimihiko Hirao. A long-range correction scheme for generalized-gradient-approximation exchange functionals. *J. Chem. Phys.*, 115(8):3540–3544, 2001. URL <https://doi.org/10.1063/1.1383587>.
- [55] Jeng-Da Chai and Martin Head-Gordon. Long-range corrected double-hybrid density functionals. *J. Chem. Phys.*, 131(17), 2009. URL <https://doi.org/10.1063/1.3244209>.

- [56] Stefan Grimme. Semiempirical hybrid density functional with perturbative second-order correlation. *J. Chem. Phys.*, 124(3), 2006. URL <https://doi.org/10.1063/1.2148954>.
- [57] Tobias Schwabe and Stefan Grimme. Towards chemical accuracy for the thermodynamics of large molecules: new hybrid density functionals including non-local correlation effects. *Phys. Chem. Chem. Phys.*, 8(38):4398–4401, 2006. URL <https://doi.org/10.1039/B608478H>.
- [58] Amir Karton, Alex Tarnopolsky, Jean-Francois Lam re, George C Schatz, and Jan ML Martin. Highly accurate first-principles benchmark data sets for the parametrization and validation of density functional and other approximate methods. Derivation of a robust, generally applicable, double-hybrid functional for thermochemistry and thermochemical kinetics. *J. Phys. Chem. A*, 112(50):12868–12886, 2008. URL <https://doi.org/10.1021/jp801805p>.
- [59]  ric Br mond, Juan Carlos Sancho-Garc a,  ngel Jos  Perez-Jim nez, and Carlo Adamo. Communication: Double-hybrid functionals from adiabatic-connection: The QIDH model. *J. Chem. Phys.*, 141(3), 2014. URL <https://doi.org/10.1063/1.4890314>.
- [60] Eric Br mond and Carlo Adamo. Seeking for parameter-free double-hybrid functionals: The PBE0-DH model. *J. Chem. Phys.*, 135(2), 2011. URL <https://doi.org/10.1063/1.3604569>.
- [61] Stefan Grimme and Frank Neese. Double-hybrid density functional theory for excited electronic states of molecules. *J. Chem. Phys.*, 127(15), 2007. URL <https://doi.org/10.1063/1.2772854>.
- [62] Marcos Casanova-P ez and Lars Goerigk. Time-dependent long-range-corrected double-hybrid density functionals with spin-component and spin-opposite scaling: A comprehensive analysis of singlet–singlet and singlet–triplet excitation energies. *J. Chem. Theory Comput.*, 17(8):51F65–5186, 2021. URL <https://doi.org/10.1021/acs.jctc.1c00535>.
- [63] Feng Yu. Spin-component-scaled double-hybrid density functionals with nonlocal van der Waals correlations for noncovalent interactions. *J. Chem. Theory Comput.*, 10(10):4400–4407, 2014. URL <https://doi.org/10.1021/ct500642x>.
- [64] Eric Bremond, Marika Savarese,  ngel Jos  Perez-Jim nez, Juan Carlos Sancho-Garc a, and Carlo Adamo. Range-separated double-hybrid functional from nonempirical constraints. *J. Chem. Theory Comput.*, 14(8):4052–4062, 2018. URL <https://doi.org/10.1021/acs.jctc.8b00261>.
- [65]  ric Br mond,  ngel Jos  Perez-Jim nez, Juan Carlos Sancho-Garc a, and Carlo Adamo. Range-separated hybrid density functionals made simple. *J. Chem. Phys.*, 150(20), 2019. URL <https://doi.org/10.1063/1.5097164>.

- [66] Frank Neese. The ORCA program system. *Wiley Interdiscip. Rev. Comput. Mol. Sci.*, 2(1):73–78, 2012. doi: 10.1002/wcms.81. URL <https://onlinelibrary.wiley.com/doi/full/10.1002/wcms.81>.
- [67] Frank Neese. Software update: the ORCA program system, version 4.0. *Wiley Interdiscip. Rev. Comput. Mol. Sci.*, 8(1):e1327, 2018. doi: 10.1002/wcms.1327. URL <https://onlinelibrary.wiley.com/doi/abs/10.1002/wcms.1327>.
- [68] Shamik Chanda and Sangita Sen. Benchmark computations of nearly degenerate singlet and triplet states of N-heterocyclic chromophores. I. Wavefunction-based methods. *J. Chem. Phys.*, 161(17), 2024. URL <https://doi.org/10.1063/5.0225537>.
- [69] Shamik Chanda, Subhasish Saha, and Sangita Sen. Benchmark computations of nearly degenerate singlet and triplet states of N-heterocyclic chromophores. II. Density-based methods. *J. Chem. Phys.*, 162(2), 2025. URL <https://doi.org/10.1063/5.0238105>.
- [70] Paul Winget and Timothy Clark. Enthalpies of formation from B3LYP calculations. *J. Comput. Chem.*, 25(5):725–733, 2004. URL <https://doi.org/10.1002/jcc.10398>.
- [71] Sambit Kumar Das, Sabyasachi Chakraborty, and Raghunathan Ramakrishnan. Critical benchmarking of popular composite thermochemistry models and density functional approximations on a probabilistically pruned benchmark dataset of formation enthalpies. *J. Chem. Phys.*, 154(4), 2021. URL <https://doi.org/10.1063/5.0032713>.
- [72] María Eugenia Sandoval-Salinas, E Brémond, AJ Pérez-Jiménez, Carlo Adamo, and Juan-Carlos Sancho-García. Excitation energies of polycyclic aromatic hydrocarbons by double-hybrid functionals: Assessing the PBE0-DH and PBE-QIDH models and their range-separated versions. *J. Chem. Phys.*, 158(4), 2023. URL <https://doi.org/10.1063/5.0134946>.
- [73] Amel Derradji, Danillo Valverde, Éric Brémond, Ángel José Pérez-Jiménez, Yoann Olivier, and Juan Carlos Sancho-García. Searching the best double-hybrid density functional to correctly predict the singlet–triplet excited-state inversion in organic systems. *J. Phys. Chem. C*, 128(43):18313–18327, 2024. URL <https://doi.org/10.1021/acs.jpcc.4c03800>.
- [74] Sebastian Kozuch, David Gruzman, and Jan ML Martin. DSD-BLYP: A general purpose double hybrid density functional including spin component scaling and dispersion correction. *J. Phys. Chem. C*, 114(48):20801–20808, 2010. URL <https://doi.org/10.1021/jp1070852>.
- [75] Lars Goerigk, Jonas Moellmann, and Stefan Grimme. Computation of accurate excitation energies for large organic molecules with double-hybrid density functionals.

- Phys. Chem. Chem. Phys.*, 11(22):4611–4620, 2009. URL <https://doi.org/10.1039/B902315A>.
- [76] Dimitrios A Pantazis. Assessment of double-hybrid density functional theory for magnetic exchange coupling in manganese complexes. *Inorganics*, 7(5):57, 2019. URL <https://doi.org/10.3390/inorganics7050057>.
- [77] Pijush Karak, Pradipta Manna, Ambar Banerjee, Kenneth Ruud, and Swapan Chakrabarti. Reverse intersystem crossing dynamics in vibronically modulated inverted singlet–triplet gap system: A Wigner phase space study. *J. Phys. Chem. Lett.*, 15(30):7603–7609, 2024. URL <https://doi.org/10.1021/acs.jpcllett.4c01437>.
- [78] Azumao Toyota. Violation of Hund’s rule in the lowest excited singlet-triplet pairs of dicyclohepta [cd, gh] pentalene and dicyclopenta [ef, kl] heptalene. *Theor. Chim. Acta*, 74:209–217, 1988. URL <https://doi.org/10.1007/BF00527144>.
- [79] Weston Thatcher Borden, Hiizu Iwamura, and Jerome A Berson. Violations of Hund’s rule in non-Kekule hydrocarbons: theoretical prediction and experimental verification. *Acc. Chem. Res.*, 27(4):109–116, 1994. URL <https://doi.org/10.1021/ar00040a004>.
- [80] Gordon A Gallup. The breakdown of Hund’s rule in systems of fourfold symmetry. *J. Chem. Phys.*, 86(7):4018–4024, 1987. URL <https://doi.org/10.1063/1.451911>.
- [81] Shiro Koseki, Takeshi Nakajima, and Azumao Toyota. Violation of Hund’s multiplicity rule in the electronically excited states of conjugated hydrocarbons. *Can. J. Chem.*, 63(7):1572–1579, 1985. URL <https://doi.org/10.1139/v85-267>.
- [82] Azumao Toyota and Takeshi Nakajima. Violation of Hund’s multiplicity rule in the lowest excited singlet–triplet pairs of cyclic bicalicene and its higher homologues. *J. Chem. Soc., Perkin trans.*, (11):1731–1734, 1986. URL <https://doi.org/10.1039/P29860001731>.
- [83] Piotr de Silva. Inverted singlet–triplet gaps and their relevance to thermally activated delayed fluorescence. *J. Phys. Chem. Lett.*, 10(18):5674–5679, 2019. URL <https://doi.org/10.1021/acs.jpcllett.9b02333>.
- [84] Johannes Ehrmaier, Emily J Rabe, Sarah R Pristash, Kathryn L Corp, Cody W Schlenker, Andrzej L Sobolewski, and Wolfgang Domcke. Singlet–triplet inversion in heptazine and in polymeric carbon nitrides. *J. Phys. Chem. A*, 123(38):8099–8108, 2019. URL <https://doi.org/10.1021/acs.jpca.9b06215>.
- [85] Marcos Casanova-Páez and Lars Goerigk. Global double hybrids do not work for charge transfer: A comment on “Double hybrids and time-dependent density functional theory: An implementation and benchmark on charge transfer excited states”. *J. Comput. Chem.*, 42(8):528–533, 2021. URL <https://doi.org/10.1002/jcc.26478>.

- [86] Roberto Peverati. Fitting elephants in the density functionals zoo: Statistical criteria for the evaluation of density functional theory methods as a suitable replacement for counting parameters. *Int. J. Quantum Chem.*, 121(1):e26379, 2021. URL <https://doi.org/10.1002/qua.26379>.

Supplementary information for:

**Leveraging the Bias-Variance Tradeoff in
Quantum Chemistry for Accurate Negative
Singlet-Triplet Gap Predictions: A Case for
Double-Hybrid DFT**

Atreyee Majumdar and Raghunathan Ramakrishnan*

Tata Institute of Fundamental Research, Hyderabad 500046, India

E-mail: ramakrishnan@tifrh.res.in

Table of Contents

1. **Dataset** Information about S_1 , T_1 and S_1-T_1 energies of twelve triangular molecules calculated with various methods.
2. **Figure S1** Error metrics for various methods using cc-pVDZ basis set
3. **Figure S2** Error metrics for various methods using cc-pVTZ basis set
4. **Figure S3** Error metrics for various methods using aug-cc-pVTZ basis set
5. **Table S1** Optimal choice of a_x and a_x for PBE-QIDH for minimizing the prediction errors for various energies
6. **Table S2** S_1 , T_1 and S_1-T_1 energies of heptazine derivatives calculated with different methods.
7. **Table S3** S_1-T_1 energy gaps of the heptazine derivatives calculated with double hybrid DFT methods and the aug-cc-pVDZ basis set.
8. **Geometries** Minimum energy geometries of HzTFEX₂, HzPipX₂, HzTFEP₂, and HzTFET₂ calculated with ω B97X-D3/def2TZVP

Dataset

S_1 , T_1 and S_1-T_1 energies of twelve triangular molecules calculated with ADC(2) and various DFT methods are collected at: <https://github.com/moldis-group/triangulenes12>. Results are presented for the cc-pVDZ, cc-pVTZ, aug-cc-pVDZ, and aug-cc-pVTZ basis sets in csv files.

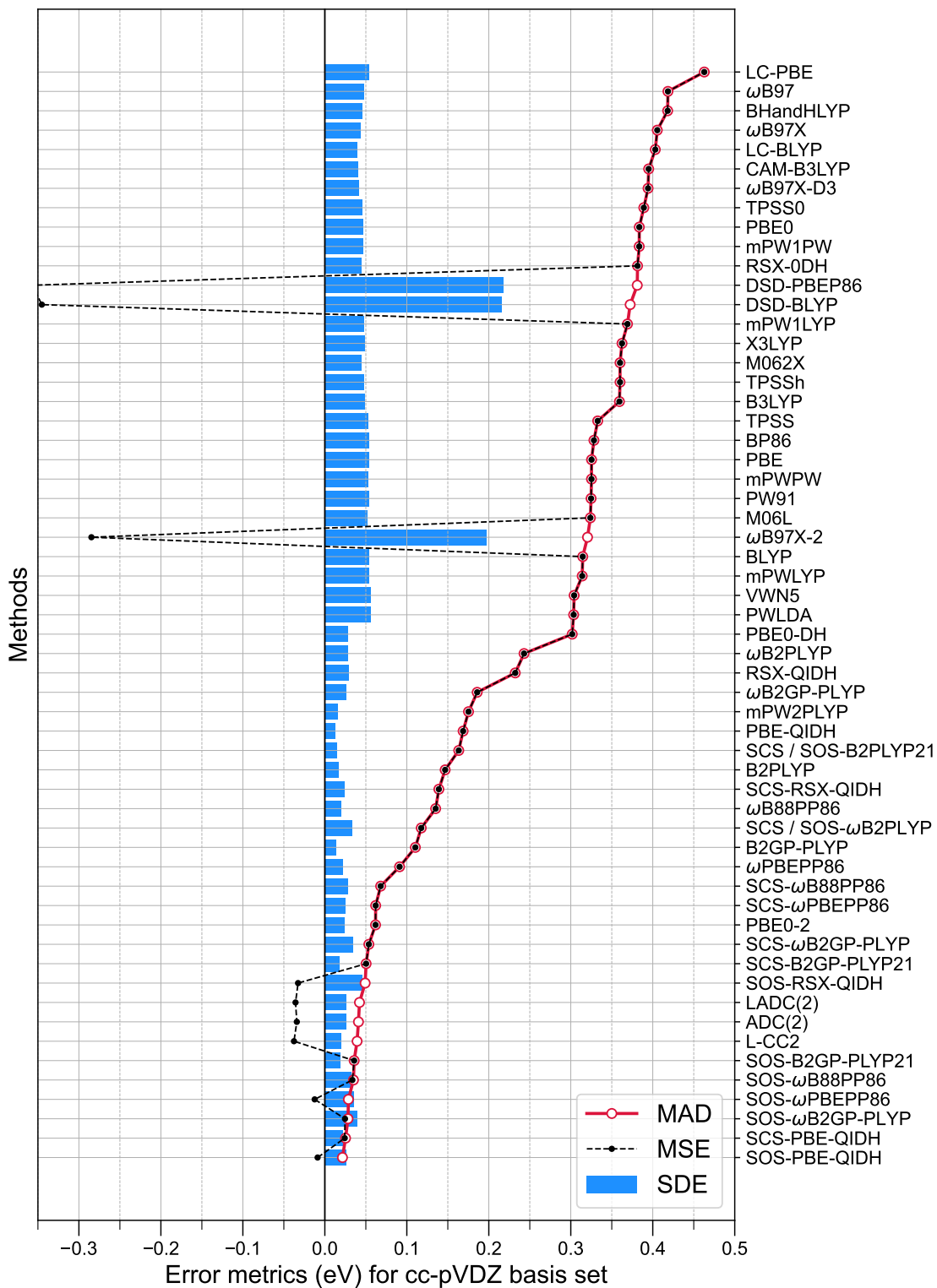


Figure S1: Error metrics for various methods with the cc-pVDZ basis set to predict 12 theoretical best estimates from Ref. 1 of STGs for triangular molecules. MAD, MSE, and SDE represent mean absolute deviation, mean signed error, and standard deviation of the error, respectively. Methods are ordered by increasing MAD, with a line included as a visual guide.

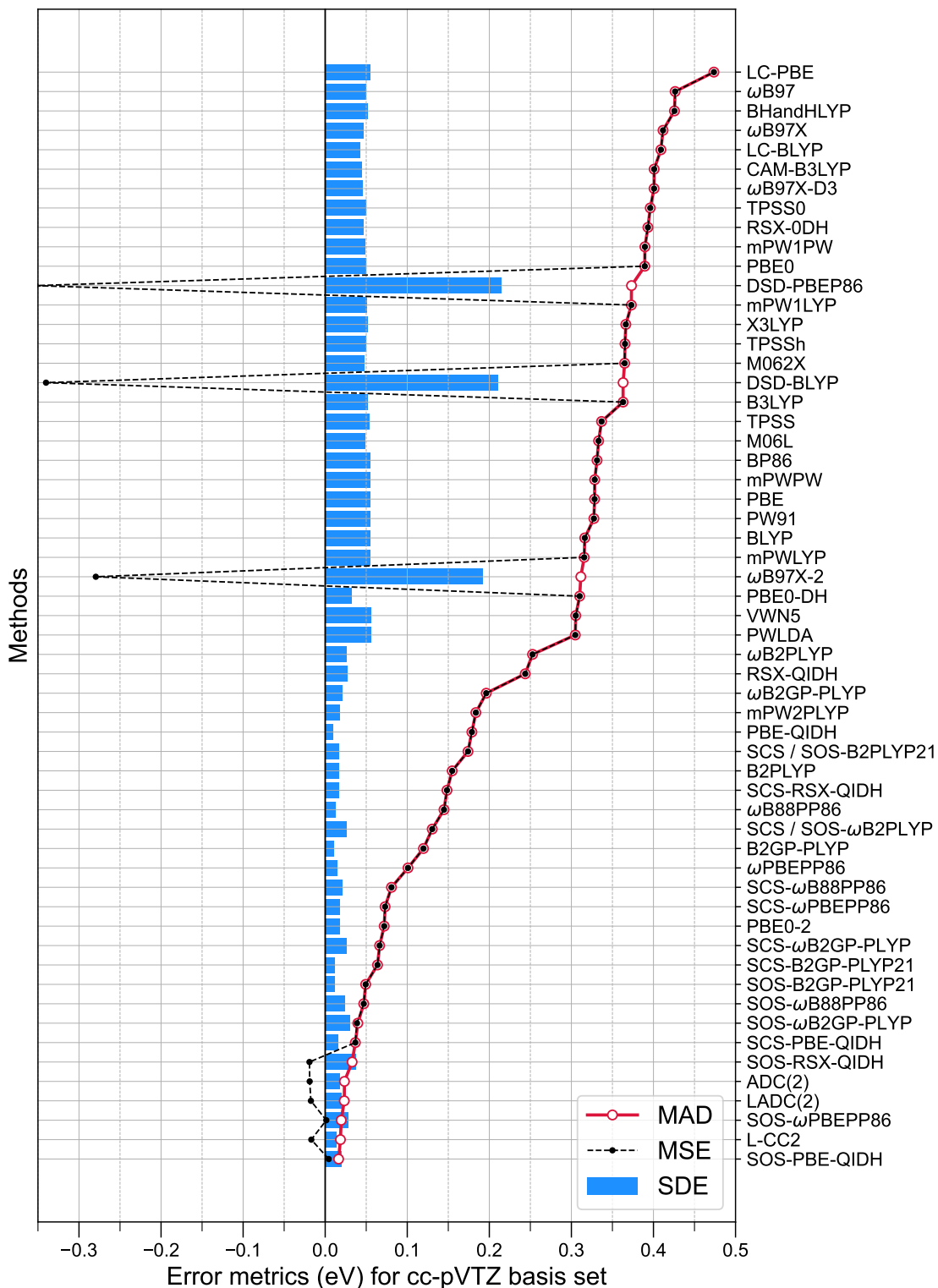


Figure S2: Error metrics for various methods with the cc-pVTZ basis set to predict 12 theoretical best estimates from Ref. 1 of STGs for triangular molecules. MAD, MSE, and SDE represent mean absolute deviation, mean signed error, and standard deviation of the error, respectively. Methods are ordered by increasing MAD, with a line included as a visual guide.

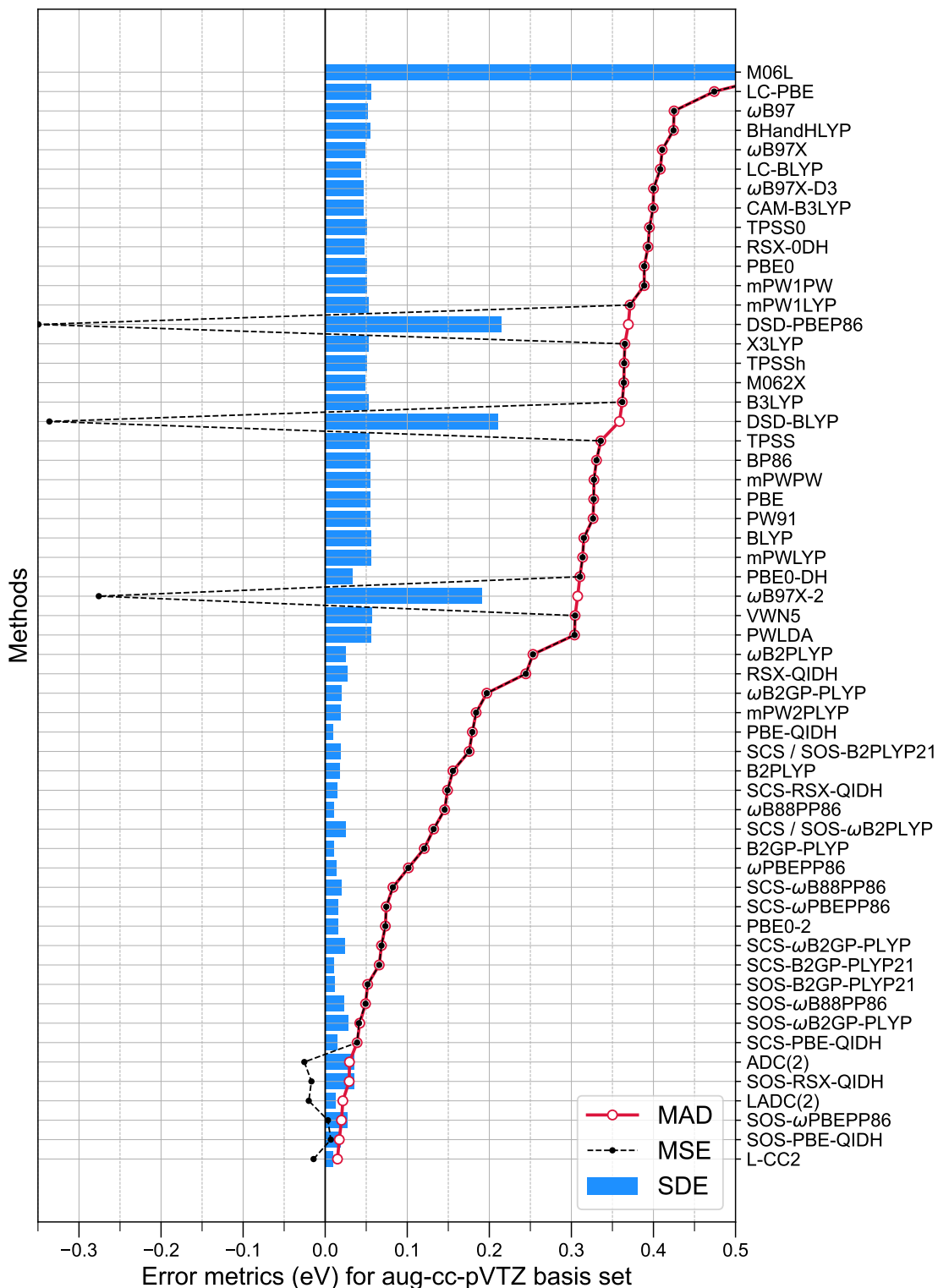


Figure S3: Error metrics for various methods with the aug-cc-pVTZ basis set to predict 12 theoretical best estimates from Ref. 1 of STGs for triangular molecules. MAD, MSE, and SDE represent mean absolute deviation, mean signed error, and standard deviation of the error, respectively. Methods are ordered by increasing MAD, with a line included as a visual guide. The high errors noted for M06L is due to de-excitations in molecules 2 and 11.

Table S1: Optimal values of a_x and a_c in Eq. (4.1) of the main article that minimize various error metrics: MSE, MAD, SDE, mean(MAD, SDE), mean(MAD, |MSE|) of various energy quantities. Also presented are values for default parameters of PBE-QIDH. Results are based on the aug-cc-pVDZ basis set.

Energy	a_x	a_c	MSE	MAD	SDE	Minimized metric
S ₁	0.85	0.80	0.002	0.080	0.093	MSE
S ₁	0.90	0.85	0.032	0.068	0.076	MAD
S ₁	0.85	0.60	0.204	0.204	0.008	SDE
S ₁	1.00	1.00	0.057	0.071	0.062	mean(MAD, SDE)
S ₁	0.85	0.80	0.002	0.080	0.093	mean(MAD, MSE)
S ₁	0.69	0.33	0.277	0.277	0.034	PBE-QIDH
T ₁	0.65	0.55	0.001	0.098	0.143	MSE
T ₁	0.50	0.15	0.007	0.022	0.030	MAD
T ₁	0.70	0.40	0.095	0.095	0.024	SDE
T ₁	0.50	0.15	0.007	0.022	0.030	mean(MAD, SDE)
T ₁	0.50	0.15	0.007	0.022	0.030	mean(MAD, MSE)
T ₁	0.69	0.33	0.100	0.100	0.033	PBE-QIDH
STG	0.50	0.45	0.001	0.073	0.101	MSE
STG	0.75	0.55	0.004	0.027	0.030	MAD
STG	0.70	0.35	0.163	0.163	0.008	SDE
STG	0.70	0.50	0.023	0.030	0.026	mean(MAD, SDE)
STG	0.90	0.65	0.001	0.029	0.034	mean(MAD, MSE)
STG	0.69	0.33	0.177	0.177	0.009	PBE-QIDH
mean(S ₁ , T ₁ , STG)	0.85	0.80	0.001	0.053	0.062	MSE
mean(S ₁ , T ₁ , STG)	0.90	0.85	0.022	0.045	0.051	MAD
mean(S ₁ , T ₁ , STG)	0.85	0.60	0.136	0.136	0.006	SDE
mean(S ₁ , T ₁ , STG)	1.00	1.00	0.038	0.047	0.042	mean(MAD, SDE)
mean(S ₁ , T ₁ , STG)	0.85	0.80	0.001	0.053	0.062	mean(MAD, MSE)
mean(S ₁ , T ₁ , STG)	0.69	0.33	0.185	0.185	0.025	PBE-QIDH

Table S2: S_1 , T_1 , and S_1-T_1 energies of heptazine derivatives shown in Figure 6 of the main article calculated with the aug-cc-pVDZ basis set.

System	Method	S_1	T_1	S_1-T_1
HzTFEX ₂	L-CC2	3.027	3.216	-0.189
	L-ADC(2)	2.933	3.133	-0.200
	B2GP-PLYP	3.115	3.247	-0.132
	PBE-QIDH	3.309	3.370	-0.061
HzPipX ₂	L-CC2	3.132	3.265	-0.133
	L-ADC(2)	3.017	3.172	-0.155
	B2GP-PLYP	3.215	3.257	-0.042
	PBE-QIDH	3.408	3.377	0.031
HzTFEP ₂	L-CC2	2.978	3.163	-0.185
	L-ADC(2)	2.887	3.079	-0.192
	B2GP-PLYP	3.081	3.188	-0.107
	PBE-QIDH	3.276	3.309	-0.033
HzTFET ₂	L-CC2	3.002	3.195	-0.193
	L-ADC(2)	2.912	3.110	-0.198
	B2GP-PLYP	3.099	3.204	-0.105
	PBE-QIDH	3.294	3.333	-0.039

Table S3: S_1-T_1 energy gaps (in eV) of heptazine derivatives shown in Figure 6 of the main article calculated double hybrid DFT methods and the aug-cc-pVDZ basis set.

System	B2GP-PLYP			PBE-QIDH		
	(65, 36)	(75, 55)	scaled ^a	(69, 33)	(75, 55)	scaled ^b
HzTFEX ₂	-0.132	-0.260	-0.262	-0.061	-0.251	-0.252
HzPipX ₂	-0.042	-0.185	-0.186	0.031	-0.176	-0.176
HzTFEP ₂	-0.107	-0.240	-0.241	-0.033	-0.231	-0.229
HzTFET ₂	-0.105	-0.243	-0.239	0.039	-0.233	-0.234

^a Calculated by scaling B2GP-PLYP (65,36) values using slope = 0.8459 and intercept=-0.1504

^b Calculated by scaling PBE-QIDH (69,33) values using slope = 0.8159 and intercept=-0.2019

EQUILIBRIUM COORDINATES (ANGSTROEM), wB97X-D3 RIJCOSX def2-TZVP
MOLECULE: HzTFEX2

CARTESIAN COORDINATES

55

Coordinates from ORCA-job geom_DFT_S0 E -1684.856743734731

C	0.20302334604288	3.17449634686885	0.01555013437540
N	-0.95310089593595	2.53069387273590	0.01091515599333
N	1.42806499495264	2.67826470260650	0.09159985163374
C	-0.89289200828159	1.20635312626344	0.09572463909890
N	0.35139255700132	0.59787400846319	0.18083085037839
C	1.51688088974707	1.36264526264511	0.17470540703940
N	2.68563116135147	0.75434187936622	0.24940454976879
C	2.70286476359846	-0.57404797189903	0.34512366723296
C	0.43586510915619	-0.78852684789517	0.27490888156087
N	1.61916273520346	-1.35780397165654	0.36573345999275
N	-1.98242392664986	0.47055405068625	0.10253290532737
C	-1.83937419119806	-0.85764149533163	0.17852275333061
N	-0.67916186684687	-1.50243230174009	0.26642101587934
C	-3.06154302137256	-1.68824893259579	0.19273015253701
C	-4.31078549477370	-1.25346290811938	-0.28823988829563
C	-5.38013047672568	-2.13952596514637	-0.19800452381296
C	-5.27292840690296	-3.41060782822038	0.34927243699315
C	-4.02698234545803	-3.82228273821900	0.81022718812541
C	-2.94333601672708	-2.97626896025679	0.72242148214650
C	-4.56844872199850	0.08386688506359	-0.92885444009523
H	-3.83834240244275	0.30831939391912	-1.70570933080145
H	-4.50029299158512	0.89205667332854	-0.20234621141229
H	-5.56304713471529	0.09011342620315	-1.37486589279926
C	-6.47119963634676	-4.31015325734967	0.45211850939721
H	-6.20620561646439	-5.34718274752903	0.24203516860818
H	-7.25580652385380	-4.00893301303150	-0.24185719524637
H	-6.88921232987692	-4.27675480253933	1.46134971546846
O	0.16889436437529	4.49581797799635	-0.06653044144381
C	-1.09973277522037	5.11359590828396	-0.16212000714530
C	-0.86136488802182	6.60721554319623	-0.24061898184402
H	-1.71502718772267	4.89836219441734	0.71146850999625
H	-1.63133045516677	4.79326552705669	-1.05826129290443
F	-0.24900814416548	7.07805928478025	0.84737702852243
F	-2.04727830426892	7.22503053852591	-0.34545415873439
F	-0.12828049365111	6.94541289665217	-1.30276811794228
H	-6.34292715955442	-1.81692458042596	-0.58057914068908
H	-1.97053643788657	-3.29898157197543	1.06748928779513
H	-3.90529295652876	-4.81220382193769	1.23515666567281
C	4.01026733884547	-1.25899508503669	0.41524871415474
C	5.23927597125098	-0.60175881231571	0.63544539899526
C	6.39106741653596	-1.38147204666917	0.65070784119513
C	4.00358846084582	-2.64494629984437	0.23400249569300
C	5.16632254551884	-3.38448603896517	0.24749183184631
C	6.38786886716241	-2.75717058699122	0.45818760660400
C	7.66784667256677	-3.54103736588975	0.50871692452208
H	7.57060723777221	-4.49391313618455	-0.01162849948922

H	7.94253734055016	-3.75601133939614	1.54451287000467
H	8.49209895686285	-2.98626784925040	0.05896681130926
C	5.40333411932219	0.87444231761120	0.87552785812487
H	6.43994887199893	1.08825641840936	1.13622704357764
H	4.75928831596937	1.22780098040934	1.67958962246429
H	5.13268535549550	1.45667705053079	-0.00388415440940
H	7.34037717052977	-0.88401123646614	0.82132002793891
H	3.05161940121683	-3.13216178194354	0.07587698033782
H	5.12473884646991	-4.45649097119782	0.09252083342269

EQUILIBRIUM COORDINATES (ANGSTROEM), wB97X-D3 RIJCOSX def2-TZVP
MOLECULE: HzPipX2

CARTESIAN COORDINATES

63

Coordinates from ORCA-job geom_DFT_S0 E -1483.952604558474

C	-0.44713295857900	3.40490930632098	-0.47888579589599
N	-1.55016234618443	2.63710546693077	-0.40858494730327
N	0.81969848832491	2.96745882164255	-0.35652798231258
C	-1.38362242310709	1.35281503360187	-0.20182246056713
N	-0.09791753429592	0.83464364143126	-0.06672599739092
C	1.00168837787759	1.68494179283999	-0.15217307524980
N	2.21957074343225	1.17248372088133	-0.02569670081121
C	2.32810897462556	-0.13265935260117	0.19784683683521
C	0.08743098759938	-0.52555178158349	0.15396670071742
N	1.31350677388118	-0.99589651559560	0.29367113909956
N	-2.41991362665298	0.52783110320955	-0.11466673036629
C	-2.17446894116598	-0.76313720707394	0.08259901333478
N	-0.96735388112756	-1.31785872005764	0.21913238129882
C	-3.33005750094123	-1.68456002196746	0.19173102980968
C	-4.60487782735169	-1.41146142737222	-0.33548074028761
C	-5.60265180864014	-2.36274463920028	-0.14053880393805
C	-5.39988896261628	-3.54896083380760	0.55088504181974
C	-4.13106913896760	-3.79914953677038	1.06106531022120
C	-3.11652898286475	-2.88558857387224	0.87145320851579
C	-4.95898693934180	-0.18018336513349	-1.12486296683895
H	-4.23130299002959	0.01931364938278	-1.91072167199605
H	-4.97340008348294	0.70664351923709	-0.49282721316861
H	-5.94073345917218	-0.30650365287011	-1.58227046366267
C	-6.50826602516157	-4.55041156629932	0.71276906604595
H	-6.46906429833363	-5.02737361048534	1.69297908702427
H	-6.42290741850317	-5.33932695617420	-0.03882680041147
H	-7.48717886661795	-4.08504652521460	0.59632184210219
H	-6.58602911390831	-2.16369420682923	-0.55458056861884
H	-2.12490520933444	-3.08427885932499	1.25470792209885
H	-3.93613513346052	-4.71564118724184	1.60665397746407
C	3.68804376566227	-0.70734123694325	0.32917194043009
C	4.83086816355784	0.04622196274995	0.66365236800017
C	6.04705464249895	-0.62240307704256	0.73275216017790
C	3.81979032070436	-2.07569903031632	0.09563168662375

C	5.04662942237368	-2.70611365045346	0.15858582279922
C	6.18628017562743	-1.98239008051708	0.47945935675191
C	7.53560952017265	-2.63815361384377	0.56212932393365
H	7.46660993418263	-3.71018977182837	0.37844235076822
H	7.98244000024637	-2.49187211481026	1.54764499096613
H	8.22228457336971	-2.21321483005167	-0.17322386740317
C	4.82368766302325	1.51607961980925	0.98696867288037
H	5.79716612002228	1.80997664378821	1.38058840590939
H	4.06066463851927	1.76352060800013	1.72439516324044
H	4.60049771828183	2.11634134841336	0.10645047181464
H	6.92960520988867	-0.05060351015199	1.00268890678904
H	2.92826513463270	-2.64066034039267	-0.14029965316483
H	5.11665078594666	-3.76978748825120	-0.03834065224320
N	-0.62484974790202	4.71435341760926	-0.68945631804556
C	0.48354127193257	5.65762200828563	-0.75430704345643
C	0.33986890203008	6.72049433346603	0.32943477580647
H	0.46518553323486	6.13014520872512	-1.74377745252671
H	1.41328528735438	5.10635895824932	-0.65850340629571
C	-1.02180892279608	7.40524633842995	0.25192061160185
H	1.14633248761920	7.44941324074002	0.22214734782550
H	0.46326674043729	6.24463461985060	1.30729844980134
C	-2.14650803643425	6.37407824499532	0.27061537554337
H	-1.08029395943477	7.98614672070157	-0.67597080665153
H	-1.14062024381680	8.11513546638070	1.07319966893884
C	-1.94463871919470	5.31915636859903	-0.81121606420308
H	-3.11637376036395	6.85476251144199	0.12415043000946
H	-2.17929925572396	5.87545060385159	1.24442477100583
H	-2.69187262386547	4.53466489840219	-0.75138070388310
H	-2.01131161768709	5.78374810611018	-1.80231672131236

EQUILIBRIUM COORDINATES (ANGSTROEM), wB97X-D3 RIJCOSX def2-TZVP
MOLECULE: HzTFEP2

CARTESIAN COORDINATES

43

Coordinates from ORCA-job geom_DFT_S0 E -1527.580180120405

C	0.26565906055690	3.07803149151747	-0.00754356320663
N	-0.89670038621008	2.44529785314390	-0.03374428327048
N	1.48324751450167	2.56874413793190	0.09556650540838
C	-0.85326175892608	1.12214170093683	0.05679494772098
N	0.38384158754145	0.49742607821141	0.16901882024982
C	1.55787019164893	1.25418813185734	0.18546325339243
N	2.71796354861820	0.63346439183619	0.29166699928863
C	2.70981254019331	-0.69465206452620	0.37875175778744
C	0.45142165490967	-0.88917141318110	0.26496136085535
N	1.62843159883136	-1.47460761962284	0.36975384606209
N	-1.95072750673439	0.39674953530922	0.04326383283794
C	-1.81655559473812	-0.92950064553683	0.14082688599885
N	-0.67077290320540	-1.59153278833633	0.24926771255518
C	-3.05762076206260	-1.73030171709231	0.12730570237934

C	-4.29649260029977	-1.10310738260713	0.01140030039890
C	-5.45565817642643	-1.85857477247314	-0.00005064810210
C	-5.38560986899717	-3.24062841522288	0.10390820382493
C	-4.15362255469965	-3.86912866871191	0.21963131975971
C	-2.99189148215687	-3.11840918495161	0.23114310065782
O	0.24790085482364	4.39811303450917	-0.09380537994009
C	-1.01109461811885	5.03273342172952	-0.21101262523115
C	-0.75070742147925	6.52342808536032	-0.27833665321838
H	-1.64475263821194	4.82200644115312	0.65036793418056
H	-1.52931608619870	4.72246490003925	-1.11839760935874
F	-0.14793202781064	6.97955249164907	0.82103883210062
F	-1.92620987946047	7.15794012668320	-0.39727750706154
F	0.00261454543809	6.85626939085996	-1.32781161025066
H	-6.41731863206651	-1.36867725259692	-0.08985118136478
H	-2.02292539389155	-3.59107191770374	0.32020528964184
H	-4.09905775408740	-4.94760233724374	0.30123290920188
C	4.02036011029041	-1.36526128419112	0.49758036348537
C	5.19134115316009	-0.60973099057827	0.50726469817021
C	6.41871527523145	-1.23803991902202	0.61829993292965
C	4.09077378836684	-2.75332803133989	0.59958543079887
C	5.32081773888610	-3.37670408117439	0.71082515124317
C	6.48460017712364	-2.62052255716330	0.72006906901298
H	7.32735017574923	-0.64886161633942	0.62511230094127
H	3.17353822520049	-3.32683041937778	0.59048951865419
H	5.37352298282244	-4.45545955772116	0.79056341691330
H	5.12064363681894	0.46667637233174	0.42656515786825
H	-4.33365970468579	-0.02495865908345	-0.06844445531037
H	7.44698068765504	-3.11095551009704	0.80664316632862
H	-6.29490929790022	-3.82991877916510	0.09527779566633

EQUILIBRIUM COORDINATES (ANGSTROEM), wB97X-D3 RIJCOSX def2-TZVP
MOLECULE: HzTFET2

CARTESIAN COORDINATES

49

Coordinates from ORCA-job geom_DFT_S0 E -1606.225000635158

C	0.24196934623939	3.06775271517226	-0.01070295723416
N	-0.91531689660199	2.42665774844494	-0.04316997873436
N	1.46304232750263	2.56854171559251	0.09510400340928
C	-0.86208021113033	1.10297531645230	0.04371172151423
N	0.37967273250662	0.48814054849041	0.15890690132316
C	1.54798793109288	1.25356809055081	0.18172003229308
N	2.71208694166478	0.64254195532668	0.29070040601397
C	2.71478585564136	-0.68700340309910	0.37540636381027
C	0.45763615525711	-0.89856459146179	0.25158523152307
N	1.63864413440587	-1.47492194771167	0.35984632318468
N	-1.95357005995202	0.37003123517973	0.02399300366241
C	-1.81023712175551	-0.95660735445898	0.11869214867936
N	-0.65879251356056	-1.60952565367959	0.22970786920639
C	-3.04257875199403	-1.76431100746071	0.09919061942170

C	-4.28943401388189	-1.15118510821137	-0.02004272427514
C	-5.43883163483182	-1.91539702945867	-0.03712443281557
C	-5.38079539965547	-3.30493373160621	0.06419648647805
C	-4.13212066795723	-3.90712891145405	0.18180377632304
C	-2.97431069949624	-3.15080727515658	0.19942440028121
C	-6.64141287565965	-4.12176331507248	0.05463653773445
H	-6.42505226724713	-5.18958169931355	0.04466703447209
H	-7.25123956935298	-3.88904653812609	-0.82035848855217
H	-7.24674709284850	-3.90807629545566	0.93839434534041
O	0.21342872288898	4.38889123956603	-0.09286867224845
C	-1.05073369734387	5.01145744752977	-0.21415445845383
C	-0.80493065882740	6.50446303396792	-0.28152420080582
H	-1.68544155349504	4.79526572142152	0.64516587660036
H	-1.56345694229829	4.69592766930734	-1.12287201644993
F	-0.21133133027726	6.96802937380558	0.81987858848747
F	-1.98625751891354	7.12753520893027	-0.40577757292515
F	-0.05077428741513	6.84445878646262	-1.32823070373210
H	-6.40308755072455	-1.42785590499186	-0.13088488190879
H	-2.00492651151503	-3.62261966877526	0.29025818123197
H	-4.06544319677551	-4.98630973829151	0.26041919583166
C	4.02696497311644	-1.34574854846863	0.49999997231080
C	5.19674946262456	-0.58619790362139	0.51589278587328
C	6.42370961230365	-1.20621337956655	0.63544587928738
C	4.11409514276588	-2.73086504505412	0.60430309078069
C	5.34929299621627	-3.34214274828739	0.72448314953917
C	6.52152804725230	-2.59327968675965	0.74258998818412
C	7.86511523373792	-3.25167773814077	0.87690072819408
H	7.77297500282554	-4.33468961151866	0.95339648040998
H	8.38558015436466	-2.89152478973167	1.76667926638815
H	8.49733539457791	-3.02437418890221	0.01608705054313
H	7.32700424911921	-0.60605367778458	0.64679113373632
H	3.20447238281058	-3.31654543792447	0.59130228083673
H	5.40518460076456	-4.42170581693613	0.80664855305162
H	5.12372965729070	0.49006751549895	0.43366247676214
H	-4.33922803345889	-0.07334757521817	-0.09901079458444

References

- (1) Loos, P.-F.; Lipparini, F.; Jacquemin, D. Heptazine, Cyclazine, and Related Compounds: Chemically-Accurate Estimates of the Inverted Singlet–Triplet Gap. *J. Phys. Chem. Lett.* **2023**, *14*, 11069–11075.